

SANDIA REPORT

SAND2002-2127
Unlimited Release
Printed July 2002

Characterization of a Track-and-Hold Amplifier for Application to a High Performance SAR

Dale F. Dubbert
Terry L. Hardin
Gilbert G. Delaplain

Prepared by
Sandia National Laboratories
Albuquerque, New Mexico 87185 and Livermore, California 94550

Sandia is a multiprogram laboratory operated by Sandia Corporation,
a Lockheed Martin Company, for the United States Department of
Energy under Contract DE-AC04-94AL85000.

Approved for public release; further dissemination unlimited.



Sandia National Laboratories

Issued by Sandia National Laboratories, operated for the United States Department of Energy by Sandia Corporation.

NOTICE: This report was prepared as an account of work sponsored by an agency of the United States Government. Neither the United States Government, nor any agency thereof, nor any of their employees, nor any of their contractors, subcontractors, or their employees, make any warranty, express or implied, or assume any legal liability or responsibility for the accuracy, completeness, or usefulness of any information, apparatus, product, or process disclosed, or represent that its use would not infringe privately owned rights. Reference herein to any specific commercial product, process, or service by trade name, trademark, manufacturer, or otherwise, does not necessarily constitute or imply its endorsement, recommendation, or favoring by the United States Government, any agency thereof, or any of their contractors or subcontractors. The views and opinions expressed herein do not necessarily state or reflect those of the United States Government, any agency thereof, or any of their contractors.

Printed in the United States of America. This report has been reproduced directly from the best available copy.

Available to DOE and DOE contractors from
U.S. Department of Energy
Office of Scientific and Technical Information
P.O. Box 62
Oak Ridge, TN 37831

Telephone: (865)576-8401
Facsimile: (865)576-5728
E-Mail: reports@adonis.osti.gov
Online ordering: <http://www.doe.gov/bridge>

Available to the public from
U.S. Department of Commerce
National Technical Information Service
5285 Port Royal Rd
Springfield, VA 22161

Telephone: (800)553-6847
Facsimile: (703)605-6900
E-Mail: orders@ntis.fedworld.gov
Online order: <http://www.ntis.gov/ordering.htm>



SAND2002-2127
Unlimited Release
Printed July 2002

Characterization of a Track-and-Hold Amplifier for Application to a High Performance SAR

Dale F. Dubbert
Synthetic Aperture Radar Department

Terry L. Hardin
RF & Optical Microsystems Department

Gilbert G. Delaplain
Synthetic Aperture Radar Department

Sandia National Laboratories
PO Box 5800
Albuquerque, NM 87185-0529

ABSTRACT

A Synthetic Aperture Radar (SAR) which employs direct IF sampling can significantly reduce the complexity of the analog electronics prior to the analog-to-digital converter (ADC). For relatively high frequency IF bands, a wide-bandwidth track-and-hold amplifier (THA) is required prior to the ADC. The THA functions primarily as a means of converting, through bandpass sampling, the IF signal to a baseband signal which can be sampled by the ADC. For a wide-band, high dynamic-range receiver system, such as a SAR receiver, stringent performance requirements are placed on the THA. We first measure the THA parameters such as gain, gain compression, third-order intercept (TOI), signal-to-noise ratio (SNR), spurious-free dynamic-range (SFDR), noise figure (NF), and phase noise. The results are then analyzed in terms of their respective impact on the overall performance of the SAR. The specific THA under consideration is the Rockwell Scientific RTH010.

ACKNOWLEDGEMENTS

This work was primarily funded under the Sandia National Laboratories LDRD (Laboratory Directed Research and Development) program. The project is entitled “Low Cost Digital Radar for Fuzing, Tags, SAR Imaging, and Targeting” and is funded under the Emerging Threats SBU.

Additional development work related to the exploitation of digital radar techniques was funded by the US National Nuclear Security Administration (NNSA), Office of Defense Nuclear Nonproliferation, Office of Nonproliferation Research and Engineering (NA-22), as the Advanced Radar Systems (ARS) project at Sandia National Laboratories. This effort is directed by Randy Bell, Project Manager, Proliferation Detection Program Office, NNSA/NA-22.

Additional Sandia personnel were instrumental in the support of this effort:

John Fuller for his phase noise characterization expertise,

Doug Greenway for his Center 1700 project leadership,

April Navarro for her test software support,

Charlie Sandoval for his test consultation, and

Pete Dudley for his development of the DRX Demo board.

CONTENTS

ABSTRACT.....	3
ACKNOWLEDGEMENTS.....	4
CONTENTS	5
1 Introduction.....	7
2 Employing a THA in the Sandia SAR	9
3 Performance Criteria for the THA	10
4 THA Measurements	11
4.1 Continuous-Time Measurements.....	13
4.1.1 DC Power.....	14
4.1.2 Linearity.....	15
4.1.3 Phase Noise (Aperture Jitter).....	17
4.1.4 Analog Bandwidth and Input/Output Impedance	20
4.1.5 CLK1 vs. CLK2 Phase Sensitivity.....	25
4.1.6 Noise Figure.....	26
4.2 Discrete-Time Measurements.....	29
4.2.1 The DRX Demo Board Acquisition System.....	29
4.2.2 Basic Test Setup.....	30
4.2.3 Linearity.....	31
4.2.4 Analog Bandwidth	35
4.2.5 Signal-to-Noise Ratio and Spurious-Free Dynamic-Range	36
4.2.6 Noise Figure.....	41
5 Analysis of THA Performance vs SAR Requirements	46
5.1 Phase Noise.....	46
5.2 Dynamic Range: Linearity vs. Noise Figure	46
5.3 SNR Degradation and SFDR.....	52
6 Summary	53
References.....	55
Matlab Scripts.....	56
FPGA Bit File.....	56

This page left intentionally blank.

1 Introduction

The Synthetic Aperture Radar (SAR) organization at Sandia National Laboratories is currently undertaking several R&D efforts towards the development of a “next-generation” miniaturized SAR or “Micro-SAR”. The goal of this collaborative effort is to realize a high performance SAR which has a total weight of approximately 20 pounds. In conjunction with the development of technology and techniques to miniaturize the critical subsystems of a SAR (such as the antenna, transmitter, processors, RF electronics, motion measurement, etc.), the digital radar technology development [1] has been identified as key to the Micro-SAR effort. Digital receiver techniques such as direct or bandpass sampling, bandwidth oversampling, and high-throughput DSP functions in field-programmable gate arrays (FPGA) show great improvement in the system performance, flexibility, and robustness, as well as significant reduction in physical size and weight.

One key element in the realization of a “true” digital radar intermediate-frequency (IF) receiver is the track-and-hold amplifier (THA). We propose that a THA plus a high-speed (1 to 1.5 GS/s), high dynamic range (8 to 10-bit) analog-to-digital converter (ADC) be employed to directly sample a 4 GHz IF signal present in our current-generation SAR systems. A simplified block diagram of the RF subsystem, showing the 4 GHz IF output, is shown in Figure 1.

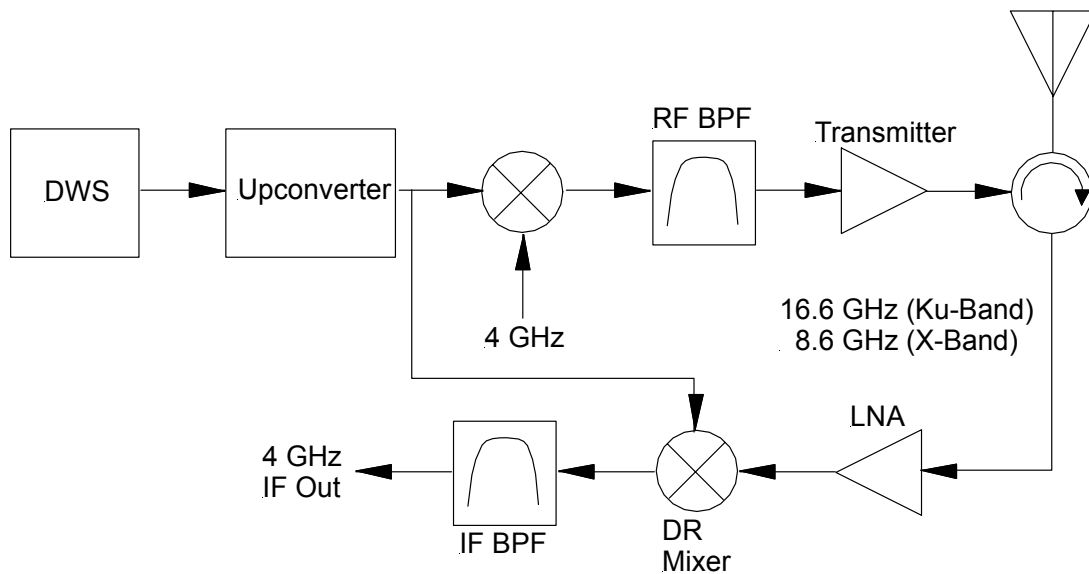


Figure 1: Simplified block diagram of the Sandia SAR RF subsystem showing the 4 GHz IF output.

A digital-waveform synthesizer (DWS) produces a linear-FM “chirped” waveform, which is up-converted to 12.6 GHz. Upper and lower sideband implementations produce wide-bandwidth (~3 GHz) transmit waveforms at Ku-band (16.6 GHz) and X-band (8.6 GHz) respectively. Because of the desired wide-bandwidth RF for fine range resolution, bandwidth compression through stretch processing is utilized. Stretch processing is a

common technique whereby the wideband RF chirp is mixed or “de-ramped” with a similar receive chirp to produce a relatively narrowband IF signal (200 to 250 MHz). It is this 4 GHz IF signal, common to all of our current SAR systems, that we wish to direct sample.

The RF to IF bandwidth compression increases the signal dynamic range at IF relative to RF. Even though the IF bandwidth of 200 to 250 MHz satisfies the Nyquist criteria for current state-of-the-art ADCs in the 1 to 1.5 GS/s range, the additional dynamic range places stringent requirements on the sampler, i.e., the THA and ADC combination.

In the classic sense, analog receiver system design employs cascade linearity (second and third-order intermodulation) and noise figure calculations based on individual component characteristics. We desire to use the same analysis for a proposed SAR receiver, which may employ a THA for direct 4 GHz IF sampling. Hence, we needed to first characterize component-level parameters such as the 1 dB gain compression, the output third-order intercept (TOI), signal-to-noise ratio (SNR), spurious-free dynamic-range (SFDR), and noise figure (NF) for the THA. In addition, time-domain jitter or phase noise degradation of the THA must be quantified to understand its potential impact to the Doppler-domain dynamic range performance of the SAR.

The purpose of this report is to document the above mentioned measurements performed on the Rockwell Scientific RTH010 [2] THA, which has been identified as a prime candidate, and possibly the only currently available candidate THA for our application. All measurement parameters and configurations are catered specifically to the direct IF sampling application mentioned. The measured data was then analyzed (some quantitative, some qualitative) to determine the general impact of the non-idealities of the THA to SAR performance.

The THA measurements in this document are specific to a proposed SAR direct IF sampling scheme. For the curious reader not familiar with SAR theory and implementation, several references including [11], [12], and [13] are available.

2 Employing a THA in the Sandia SAR

In Figure 2, we show how the THA might be employed to direct sample the SAR 4 GHz IF output.

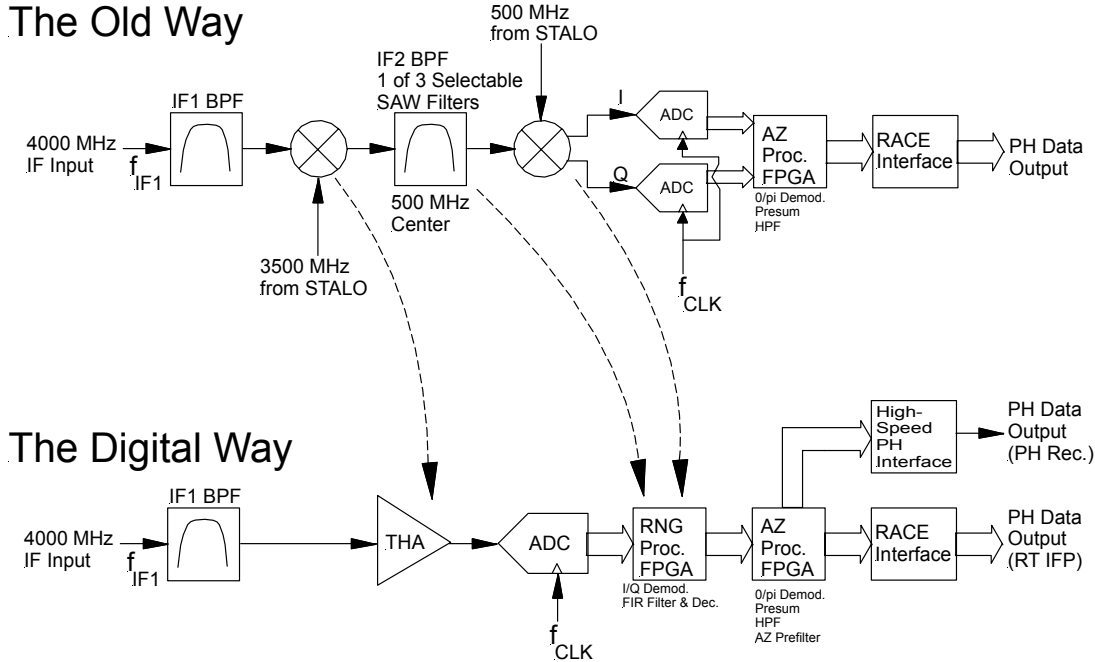


Figure 2: Comparison of simplified block diagrams for the current SAR IF configuration and the proposed digital IF implementation employing a fast THA.

The “Old Way” shows the current implementation. Currently, analog down-conversion, analog IF filtering using surface-acoustic wave (SAW) filters, and analog quadrature (I/Q) demodulation are employed. The “Digital Way” performs the necessary frequency conversion by direct sampling the IF using the THA and the ADC. IF filtering and quadrature demodulation, amongst other DSP operations, are all performed in FPGAs.

We are currently developing a digital IF receiver module upgrade to our current SAR. This module utilizes bandwidth over-sampling and high-throughput DSP functions in FPGAs. However, we have chosen not to employ a THA to direct sample the IF. Instead, classic analog down-conversion is employed due to its lower implementation risk. Future radars developed at Sandia National Labs may very well employ the benefits of direct sampling using a THA, assuming that the device meets the system performance requirements.

3 Performance Criteria for the THA

Here, we review the measurements we have performed on the THA and briefly discuss, in a qualitative sense, why they are important to the overall SAR performance.

DC Power

In a Micro-SAR application, DC power consumption and thermal management is of concern for any component.

Linearity

We measure both the 1 dB gain compression point and the third-order intercept (TOI) to gauge the impact of the THA on the linearity performance of the SAR. Ideally, we want the intermodulation contributions of all components in the receiver to meet a certain maximum acceptable level when a maximum signal level is present at the ADC input. This basically determines the upper-end of the overall system dynamic range performance.

Phase Noise

Since the SAR employs Doppler or pulse-to-pulse processing to resolve objects in the cross-range dimension, phase noise must be minimized to ensure adequate SNR in the final SAR image. The primary phase noise contributor in a SAR is the reference oscillator. However, the sampler (THA and ADC) can potentially be a significant contributor to the system phase noise.

Analog Bandwidth

The THA must certainly support the 4 GHz direct IF sampling application. In addition, we wish to measure the gain of the THA vs. frequency to assess the possibility of using the RTH010 for future direct sampling applications up to X-band frequencies.

Clock Phase Sensitivity

Since the RTH010 employs a two-stage THA with separate clock inputs (CLK1 and CLK2), we wish to observe the sensitivity of the linearity performance (namely 1-dB gain compression) relative to the phase between CLK1 and CLK2.

Noise Figure

The noise figure performance of the THA at 4 GHz helps determine the lower limit of the SAR dynamic range.

SFDR and SNR

Both SFDR and SNR are measured and compared to the same parameters for the ADC itself. Since the ADC is typically the dynamic range “bottleneck” in a SAR employing stretch processing, we want to carefully assess the effective number of bits (ENOB) of the THA and ADC as compared to the ADC alone.

4 THA Measurements

The RTH010 is actually a two-stage THA operating at a maximum clock frequency of 1 GHz. Each stage has its own differential clock input as shown in Figure 3. For all THA tests outlined in this document, CLK1/CLK1B and CLK2/CLK2B are driven from the same clock source through 180° hybrid couplers.

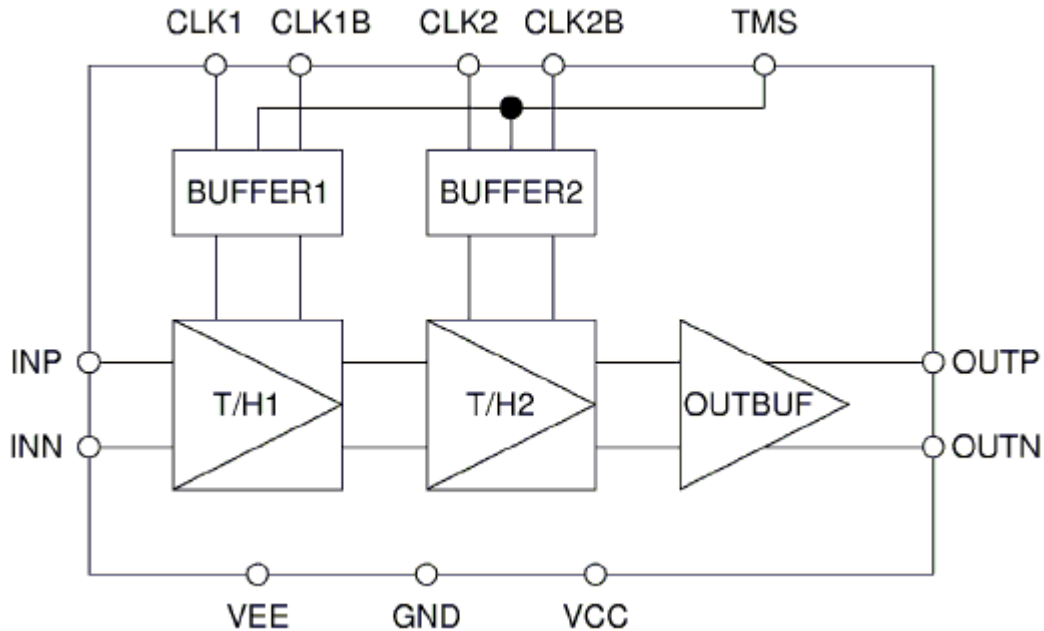


Figure 3: Operational diagram of the RTH010 THA.

For most tests performed on the THA, the basic test setup shown in Figure 4 was used. The one exception was the discrete-time test, where the output 180° hybrid coupler was not used. The RTH010 THA was mounted on a Rockwell Scientific RTH010 evaluation board. Most of the tests were performed with differential input and output, and a nominal clock frequency of 1 GHz as shown in Figure 4. A photograph of the THA test brass-board, with the output coupler removed, is shown in Figure 5. Refer to the data sheet [2] for more information on the operation of the RTH010.

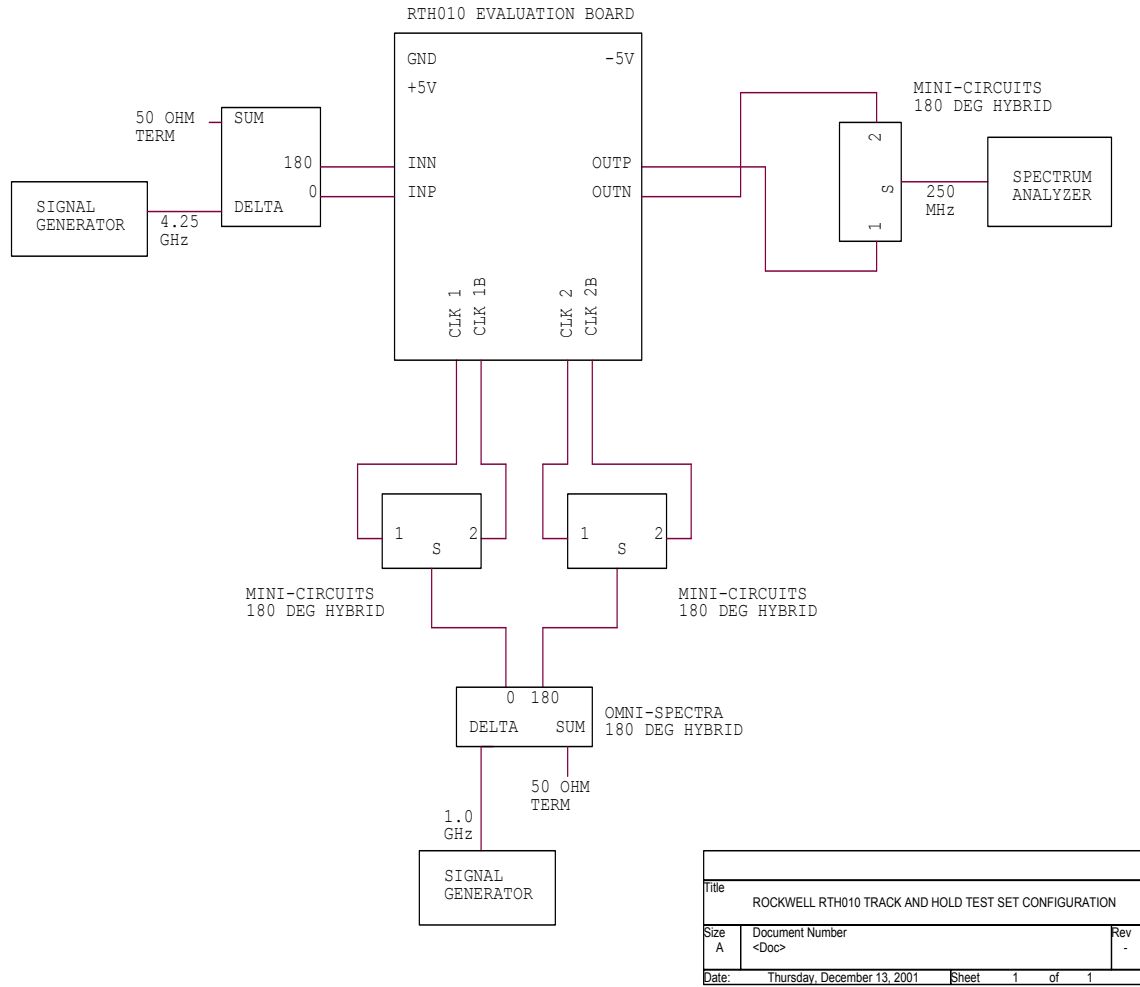


Figure 4: Basic setup for testing the THA.

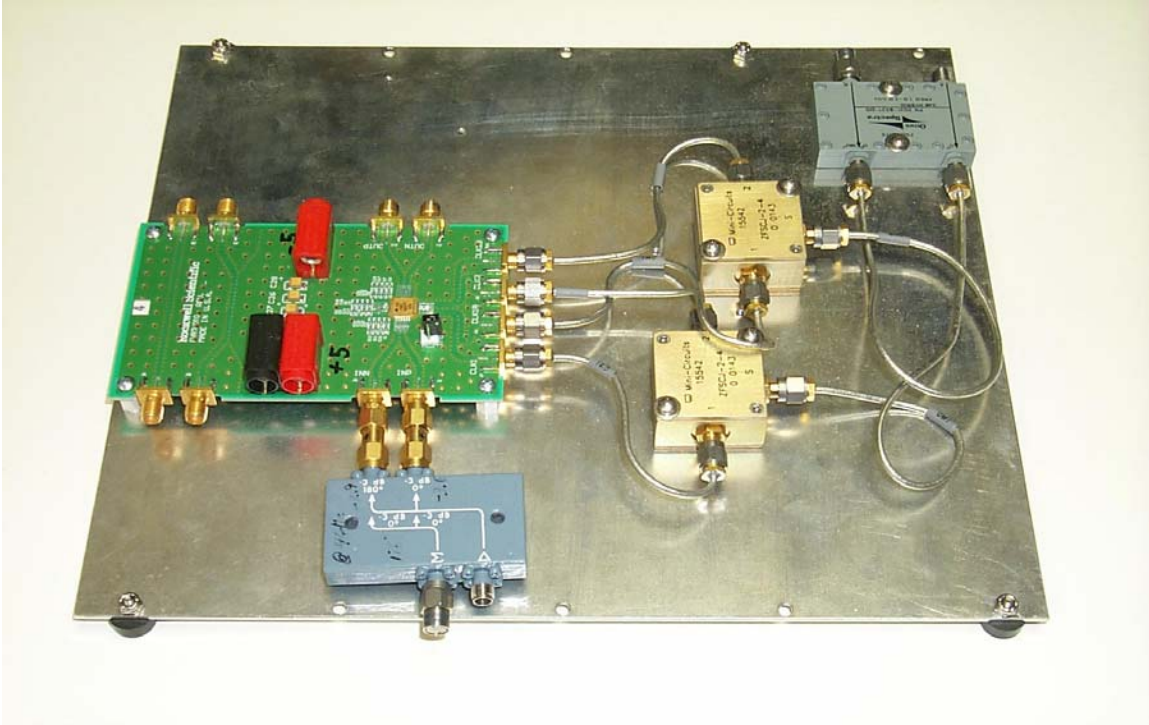


Figure 5: Photograph of RTH010 evaluation board with RF and clock hybrid couplers.

4.1 Continuous-Time Measurements

Classically, analog components are all measured using continuous-time measurement equipment. In other words, measurements such as noise figure, spectral output vs. input power, and phase noise all involve measurements which are continuous-time integrals. The THA is a different category of hardware. It is neither an analog component in the truest sense, nor is it a purely discrete component. Therefore, the validity of certain continuous time measurements performed on a THA is in question.

In any digital receiver application, an ADC will follow the THA. The ADC samples the THA output during the THA hold period. It can be argued that all parameters (noise, linearity, phase noise, etc.) must be measured with an ADC such that only data during the hold phase is collected. This stands to reason. However, we chose to perform measurements for noise figure and linearity using both continuous and discrete-time techniques for the purpose of investigation.

In general, we found that the linearity measurements (1 dB compression and TOI) were in very good agreement between the continuous and the discrete-time measurements. Noise figure, on the other hand, was much higher for the continuous-time measurement. This places doubt on the validity of measuring THA output noise using a continuous-time measurement system.

4.1.1 DC Power

The DC power consumption of the RTH010 was measured as follows:

+5.00v @ 0.125 A (0.625 W),
-5.00v @ 0.291 A (1.455 W),
2.08 Watts Total DC Power Input.

This is a significant amount of power dissipation for such a small device. However, the RTH010 mounted on the evaluation board did not pose any thermal problems since a good thermal interface was provided between the bottom of the package and the ground plane of the board.

4.1.2 Linearity

For a truly linear amplifier, the output power is a linear function of the input power. A linear amplifier produces, at its output, an amplified and delayed replica of the input signal with negligible or no harmonic generation. Here we perform both a 1 dB gain compression and third-order intercept measurement to determine the linearity of the THA.

The 1dB compression point calculations for the following data compensate for the 180° hybrid couplers so that the data reflects the THA results only. We found that the 1 dB compression point was -2.1 dBm at the THA output (see Figure 6).

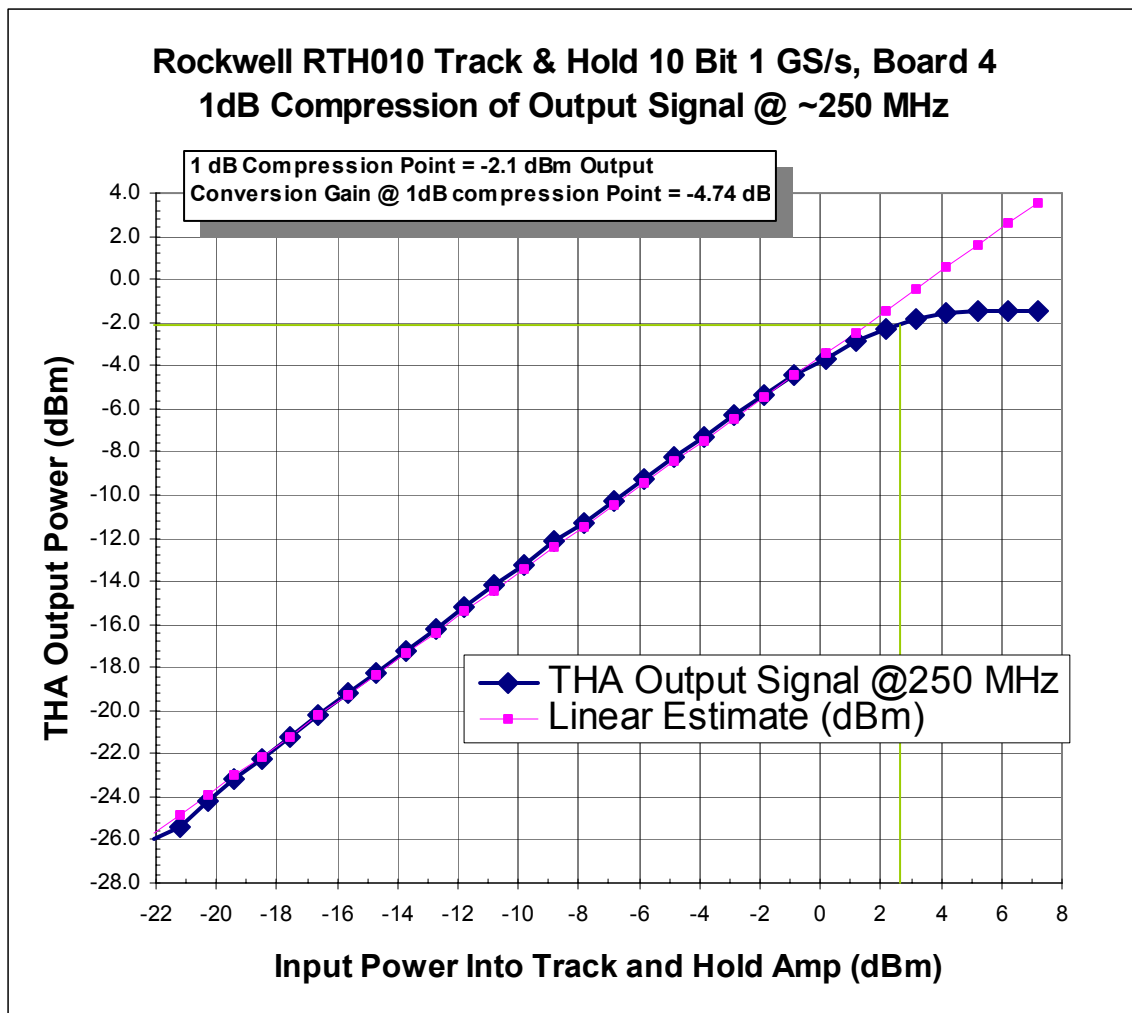


Figure 6: Output vs. Input Power and 1-dB gain compression for the THA.

The Two-Tone Third-Order Intercept Point (*TOI*) is a measure of the third-order intermodulation products generated by two sine-waves at the input of the device. By

measuring the output power at the intersection of linear extrapolations of the fundamental and intermodulation output powers vs. input power, we can determine the intermodulation level I_3 (dBc). This is determined by

$$I_3 = 2(P_0 - TOI), \tag{1}$$

where P_0 is the output power (dBm) in a single fundamental tone, and TOI is the output power (dBm) at the intersection of the fundamental and intermodulation linear curves.

The third Order Intercept Point calculations for the following data compensate for the 180° hybrid couplers so that the data reflects the THA only. We found that the TOI Point was +5.5 dBm at the THA output (see Figure 7).

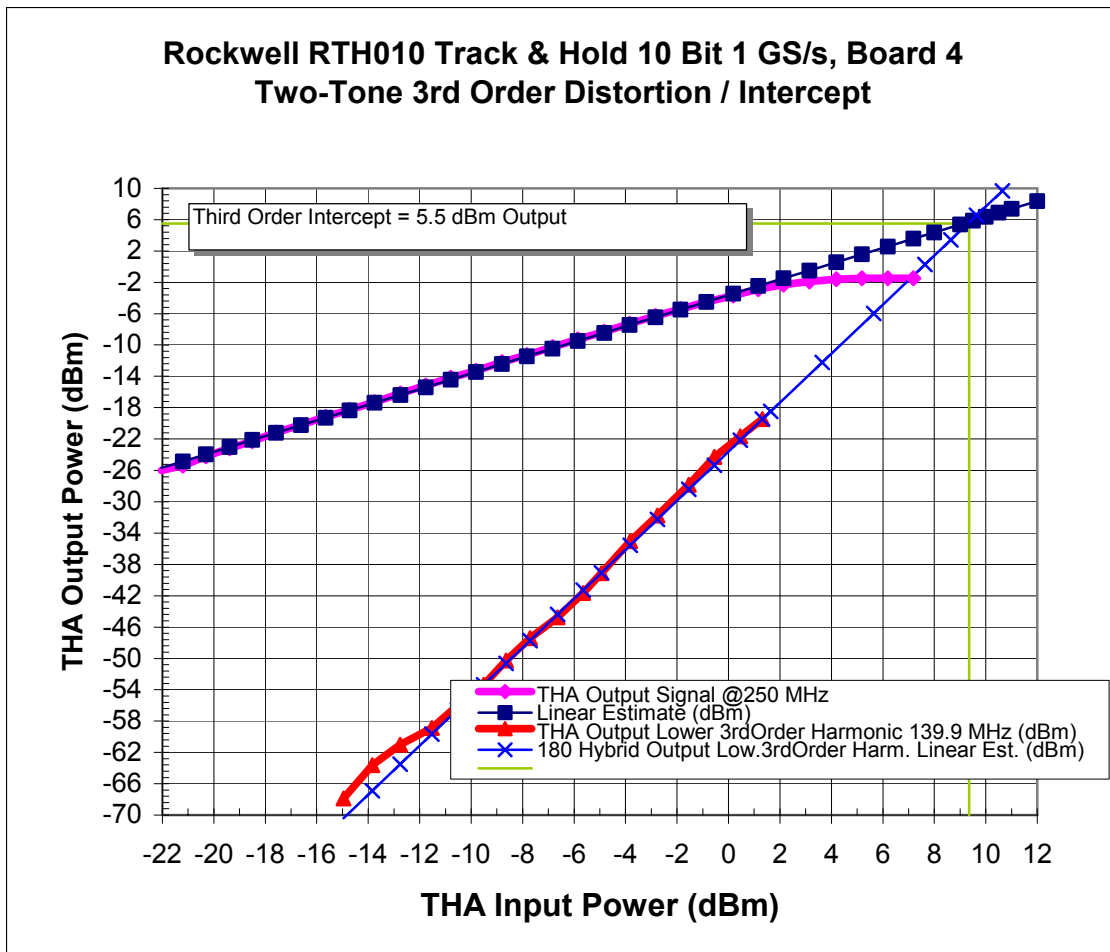


Figure 7: Two-tone output vs. input power and TOI measurement.

4.1.3 Phase Noise (Aperture Jitter)

The purpose of this measurement was to characterize the single-sideband (SSB) residual phase noise of the THA using the HP (Agilent) E5500 phase noise measurement system [3]. Figure 8 shows the test setup for measuring the residual phase noise of the THA using the HP E5500. It is assumed that the residual phase noise of the diode mixer is negligible. The clock source (1000 MHz) is of the low phase noise variety (HP8662A). The line stretcher facilitates calibration of the phase detector constant. The noise floor of the setup was also measured by inserting another diode mixer in place of the DUT as shown in Figure 8. The noise floor measurement also confirms the assumption that the residual phase noise of the diode mixer is negligible.

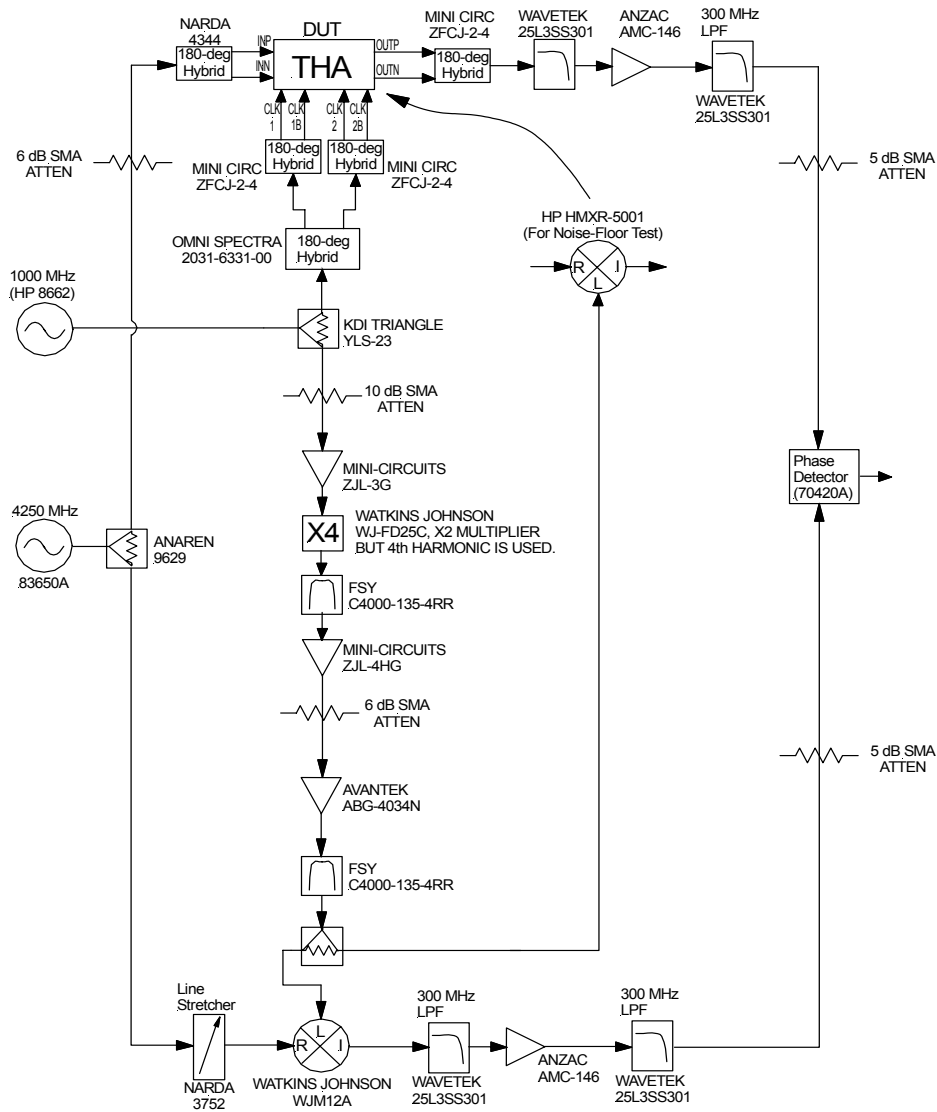


Figure 8: Phase noise test setup.

With a 1 GHz clock frequency, a 4235 MHz RF input was chose to produce a 235 MHz IF output. This IF frequency was chosen (instead of 250 MHz) to eliminate unwanted spurious signals in the phase noise spectrum.

A fundamental figure of merit for the aperture stability of the THA is the total RMS phase noise, which can be directly related to RMS timing jitter. We can begin with the integrated sidelobe ratio (*ISLR*) which is calculated by integrating the relative magnitude SSB phase noise \mathcal{L} over a specified minimum (*fmin*) and maximum (*fmax*) offset frequency:

$$ISLR = 10 \log_{10} \left[2 \int_{f_{\min}}^{f_{\max}} |\mathcal{L}| df \right], \quad (2)$$

where \mathcal{L} is the magnitude SSB phase noise and is determined from the phase noise in dB (\mathcal{L}_{dB}) by

$$\mathcal{L} = 10^{\left(\frac{\mathcal{L}_{dB}}{10} \right)}. \quad (3)$$

We typically integrate the phase noise from 100 Hz (*fmin*) to 20 MHz (*fmax*).

The total RMS phase noise (ϕ_{RMS}) in degrees is

$$\phi_{RMS} = \left(\frac{180}{\pi} \right) 10^{\left(\frac{ISLR}{20} \right)}. \quad (4)$$

A Matlab program was used to perform the above calculations on the HP E5500 output data.

The RTH010 data sheet [1] specifies the total RMS timing jitter Δt_{RMS} which is related to ϕ_{RMS} as

$$\Delta t_{RMS} = \frac{\phi_{RMS}}{360 f_{RF}}, \quad (5)$$

where f_{RF} is the THA input frequency (4235 MHz in this case).

It is interesting to note that the RTH010 data sheet [2] advertises a 0.1 psec aperture jitter. We assumed that this is an RMS number, even though it is not specified in the data sheet. This equates to a total RMS phase noise of 0.15° RMS and an ISLR of -51.5 dB. This is very small but should be measurable using the HP E5500.

The results of the SSB phase noise measurement of the THA are shown in Figure 9.

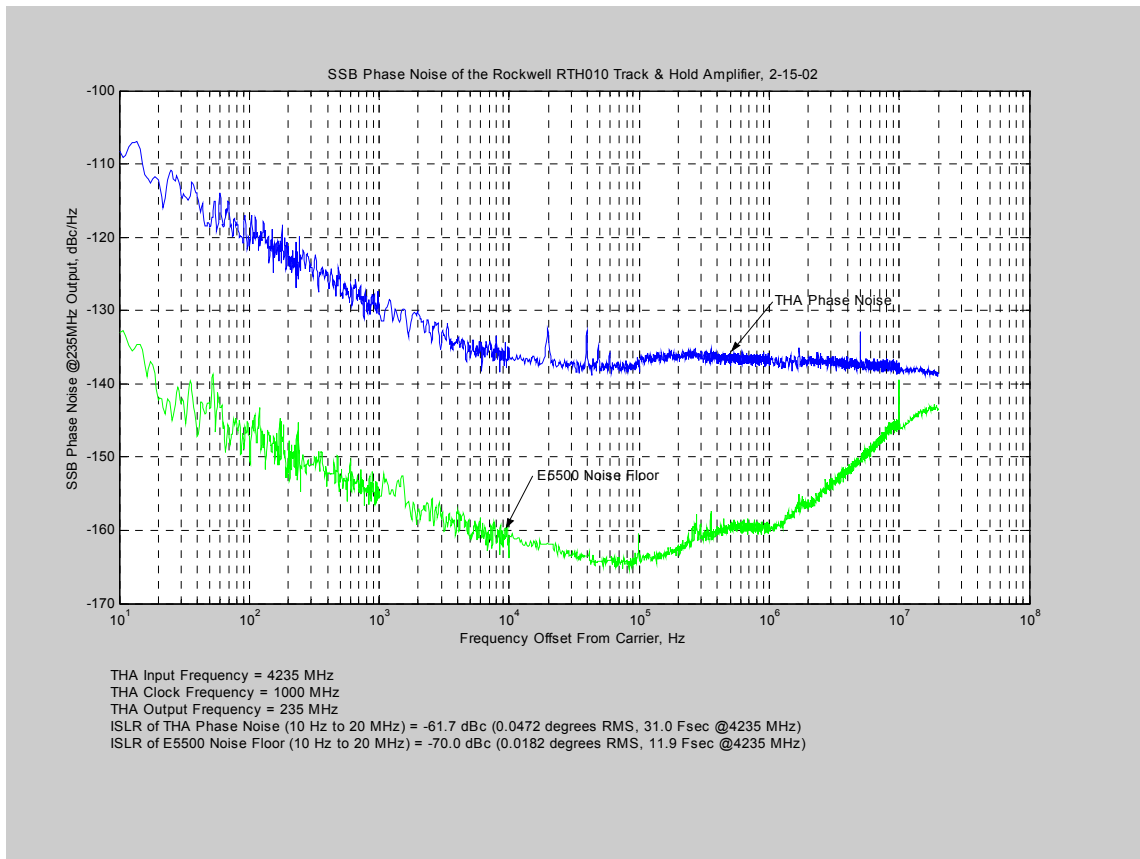


Figure 9: Results of the SSB phase noise measurement for the THA.

From the SSB phase noise vs. frequency plot of Figure 9, we make the following observations:

- The noise floor of the E5500 test setup is significantly lower than the THA phase noise, which helps to validate the phase noise measurement.
- The integrated phase noise is calculated from equation (2) as -61.7 dBc, which equates to a total RMS phase noise (equation (4)) of 0.0472° , or a total RMS time jitter (equation (5)) of 0.031 psec at 4235 MHz. This is a very low phase noise contribution as discussed in more detail in section 5.1.
- We notice that the noise floor is relatively flat for carrier offsets > 10 kHz. If this is due to a phase noise contribution, then the total integrated phase noise could be significant if we integrate it over a larger bandwidth. However, we believe that this is due to the thermal noise floor of the device, suggesting that the THA has a high inherent noise figure.

We can calculate an estimate for the noise figure of the THA based on the relative noise power spectral density (PSD) as:

$$F_{THA} \cong \frac{P_o L}{k T G_{THA}}, \quad (6)$$

where P_o is the signal power at the THA output, k is Boltzman's constant (1.38×10^{-23} Wsec/K), T is the absolute temperature (298 °K), and G_{THA} is the gain of the THA (approximately -3 dB). Assuming $\mathcal{L}_{dB} = -138$ dBc/Hz, $P_o = -5$ dBm, we calculate the noise figure estimate as

$$F_{THA} \cong 34 \text{ dB.}$$

As we will see in section 4.1.6, this is in close agreement with the continuous-time noise figure measurement. We do warn that the results of the discrete-time noise figure measurement of section 4.2.6 strongly suggest that the measurement of THA noise figure in the continuous-time domain is not a valid measurement.

4.1.4 Analog Bandwidth and Input/Output Impedance

We found that the output response was not very flat over the band of DC to 7GHz when measured in the continuous-time domain. Therefore we were prompted to look at the input and output impedance of the THA and the input impedance of the 180° hybrid coupler. We found that this variation in the output response was due primarily to the impedance variation of the hybrid coupler (or balun) and the THA:

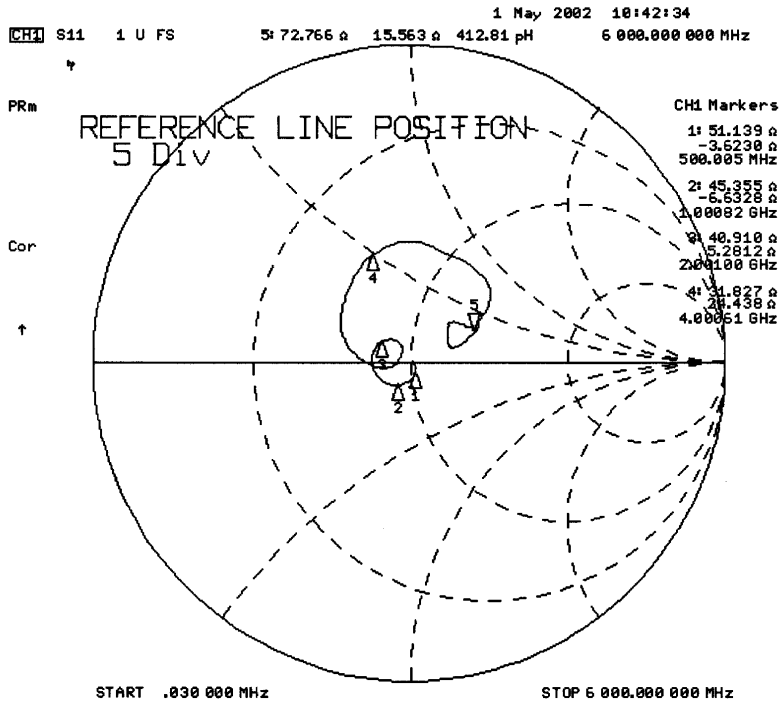
- The input impedance of the THA varies from 51.85 (at 500 MHz) to 37.96 (at 4 GHz) to 74.50 (at 6 GHz) ohms.
- The output impedance of the THA varies from 34.76 (at 50 MHz) to 54.94 (at 450 MHz) ohms.
- The input impedance of the 180° hybrid coupler varies from 48.47 (at 50 MHz) to 100.10 (at 450 MHz) ohms.
- We also tried a balun on the THA output in place of the 180° hybrid coupler. The results were similar, due to the input impedance of the balun varying from 23.23 (at 50 MHz) to 69.37 (at 400 MHz) to 53.24 (at 500 MHz) ohms.

The combination of these changes in impedances caused the output to vary greatly over the broad input bandwidth.

For the record, the input and output impedance, displayed both on the Smith chart and as log magnitude, are shown in Figure 10, Figure 11, Figure 12, and Figure 13.

We chose to abandon the continuous-time bandwidth measurement in favor of the discrete-time measurement (section 4.2.4). The later does not require an output hybrid coupler or balun, so the aforementioned impedance problem is avoided.

THA INP



THA INP

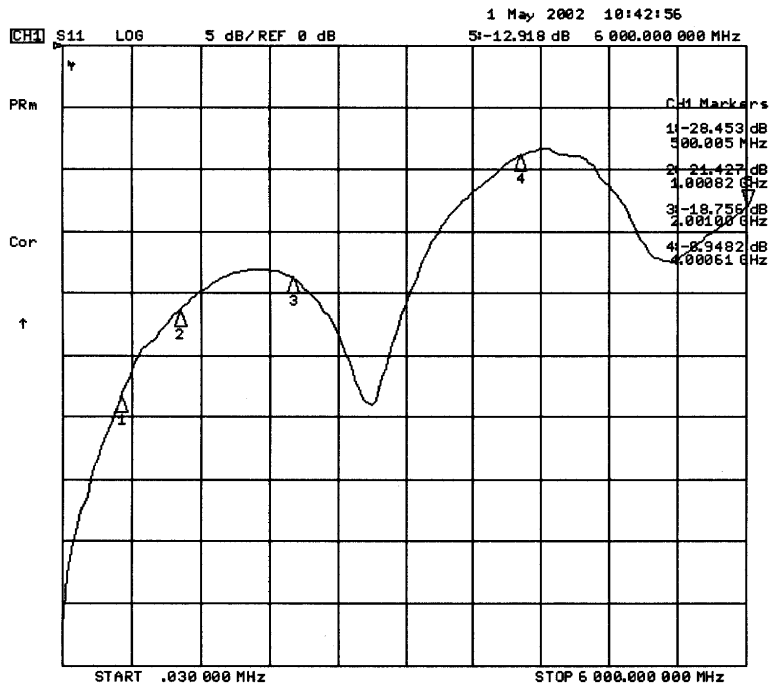
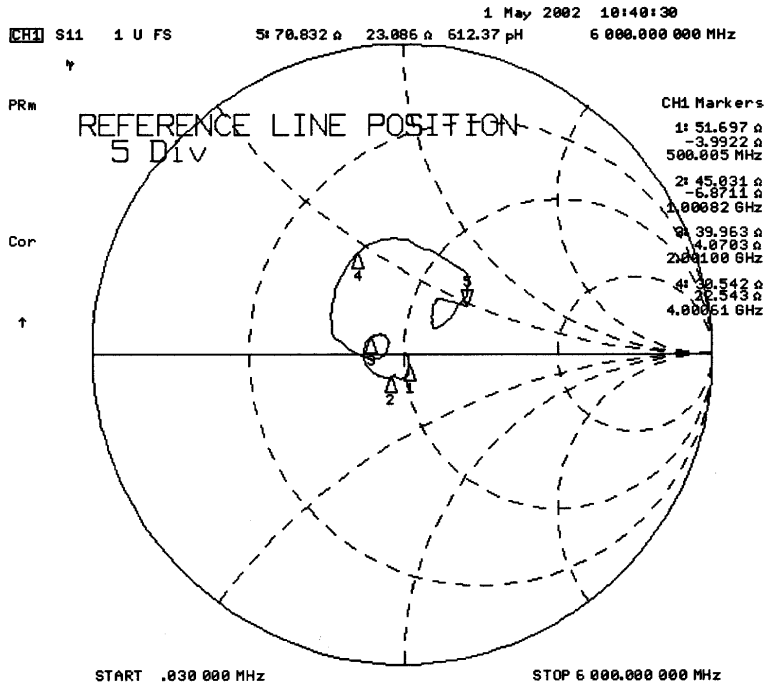


Figure 10: THA input impedance, positive port.

THA INN



THA INN

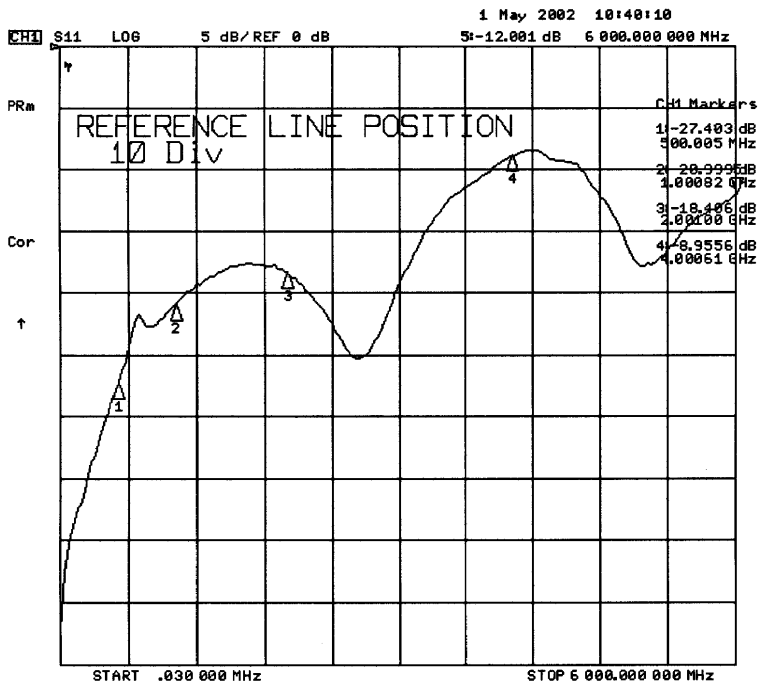
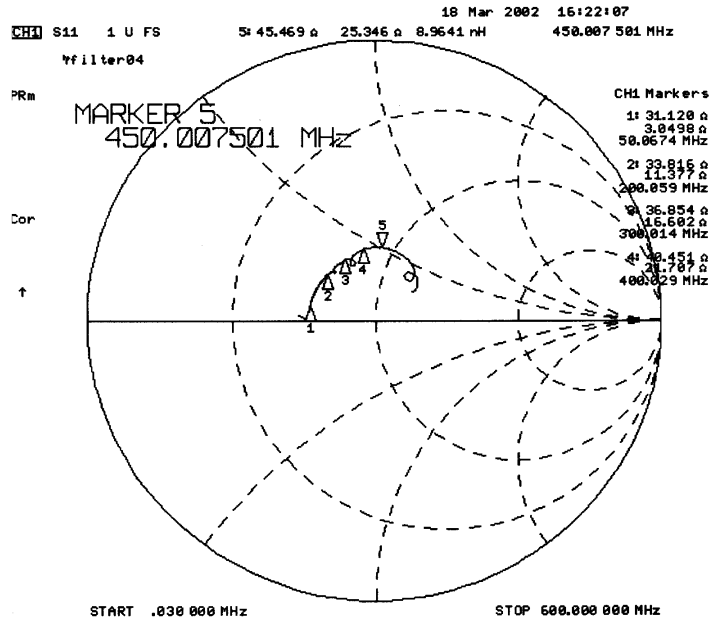


Figure 11: THA input impedance, negative port.

THA OUTP



THA OUTP

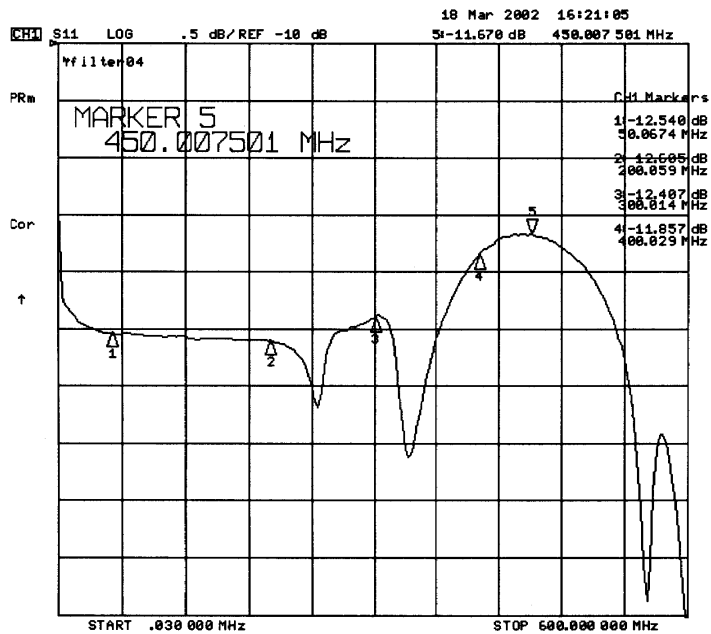
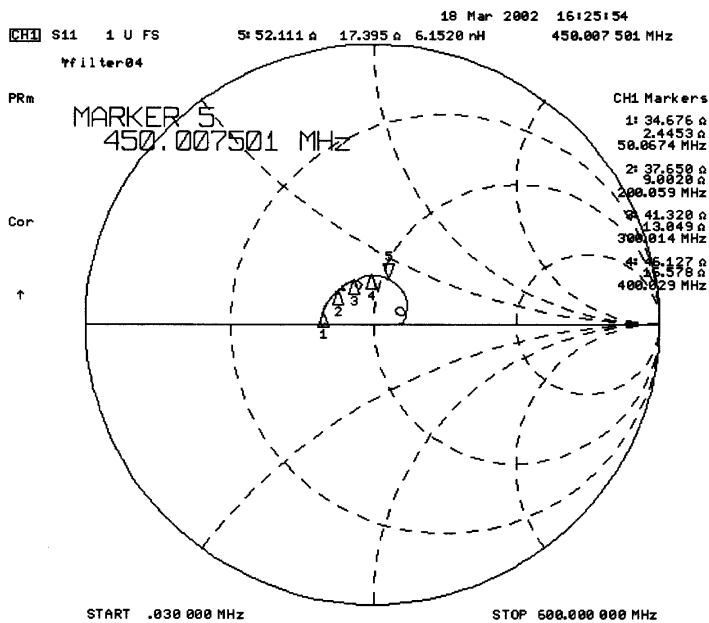


Figure 12: THA output impedance, positive port.

THA OUTN



THA OUTN

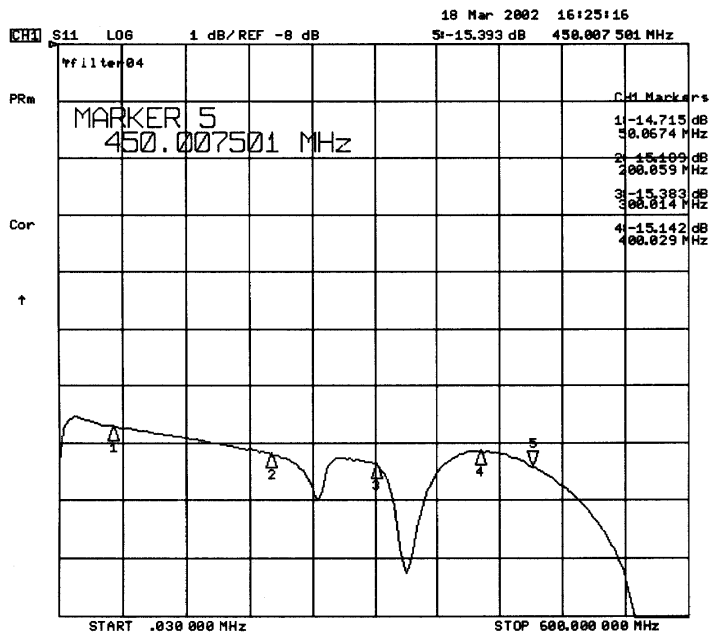


Figure 13: THA output impedance, negative port.

4.1.5 CLK1 vs. CLK2 Phase Sensitivity

In this measurement, we were interested in the effect on THA linearity performance when the phase relationship between CLK1 and CLK2 was varied. The specific linearity performance parameter chosen for this measurement was the 1 dB gain compression output power. Normally, the CLK1/CLK2 phase is 180°. In Figure 14, we show the variation of the 1 dB compression point vs. CLK1/CLK2 phase relative to 180°. We note that the data includes the phase error of the 180° hybrid couplers. However, the phase errors of the couplers were found to be relatively small as compared to the clock phases. Note also that the data includes the insertion loss of the input and output couplers, which results in higher absolute 1 dB compression values.

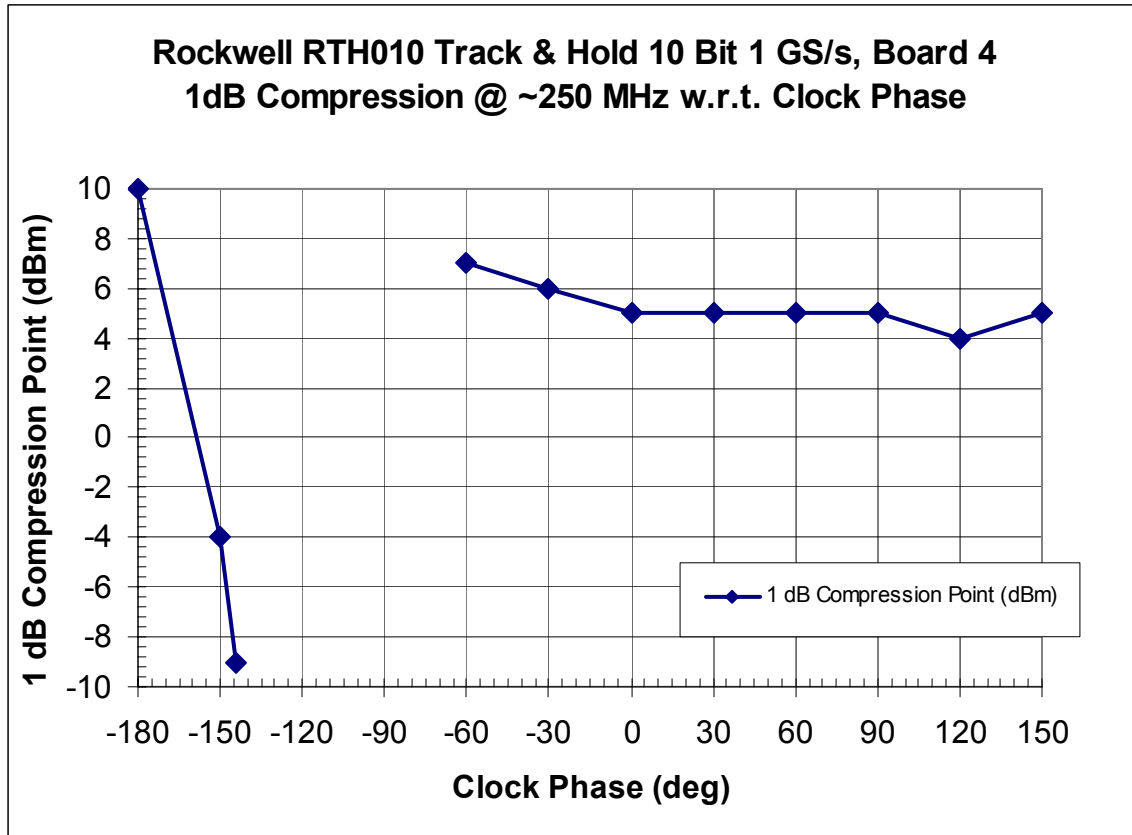


Figure 14: Measurement of 1 dB output compression point vs. clock phase.

Note that the 1 dB compression point is relatively insensitive to the clock phase over most of the range. The data was taken at 30° intervals. The data points at -90° and -120° are outside of the hold interval of the THA so are omitted. If anything is to be learned from the results of Figure 14, it is that if we are to error in the CLK1/CLK2 phase relationship (relative to 180°), it should be a positive error.

4.1.6 Noise Figure

Here we use the standard “Y-factor” technique to measure the noise figure of the THA in continuous-time. The Y-factor is simply the ratio of the system output noise power with the noise source on (hot) to that with the noise source off (cold). The noise figure of the device is calculated from the Y-factor and the noise source excess noise ratio (*enr*) as

$$F = \frac{enr}{Y - 1}. \quad (7)$$

Because of the relatively high expected noise figure of the THA, a preamplifier is needed to essentially increase the ENR of the noise source. A bandpass filter on the THA input assures that noise only appears in the 4 GHz IF band of interest. Due to the relatively high noise floor of the spectrum analyzer, we also include gain (2-stage post-amplifier) after the THA to assure that the analyzer input noise with the noise source off is at least 15 to 20 dB above the analyzer noise floor.

We also note that the THA gain and noise figure in the calculations to follow include the loss of the input and output couplers.

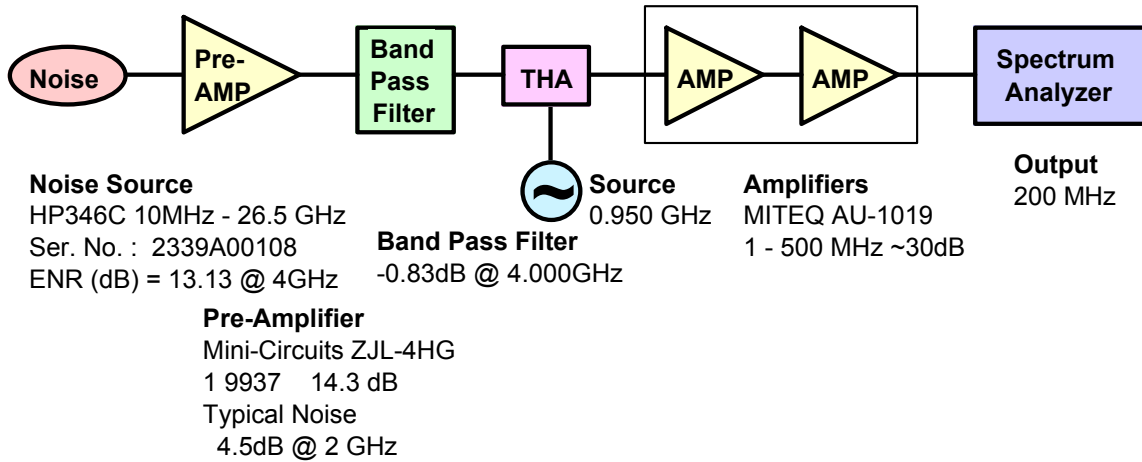


Figure 15: Test setup for the continuous-time noise figure measurement.

Here we derive the equivalent excess noise ratio (*enr*) of the noise source consisting of the noise source itself (subscript NS), the preamp (subscript PA), and the bandpass filter (subscript FILT).

Total Output Noise of the Noise Source Chain with Noise Source "Hot":

$$\begin{aligned} N_{HOT} &= kTB G_{PA} G_{FILT} + (f_{NS} - 1) kTB G_{PA} G_{FILT} + (f_{PA} - 1) kTB G_{PA} G_{FILT} + (f_{FILT} - 1) kTB G_{FILT} \\ &= kTB G_{FILT} [G_{PA} + (f_{NS} - 1) G_{PA} + (f_{PA} - 1) G_{PA} + (f_{FILT} - 1)] \\ &= kTB G_{FILT} \{G_{PA} [1 + (f_{NS} - 1) + (f_{PA} - 1)] + (f_{FILT} - 1)\} \\ &= kTB G_{FILT} \{f_{FILT} - 1 + G_{PA} [1 + f_{NS} - 1 + f_{PA} - 1]\} \\ &= kTB G_{FILT} \{f_{FILT} - 1 + G_{PA} [f_{NS} + f_{PA} - 1]\} \\ &= kTB G_{FILT} G_{PA} \{f_{NS} + f_{PA} - 1 [(f_{FILT} - 1) / G_{PA}]\}. \end{aligned}$$

Total Output Noise of the THA Input Terminated (Noise Source "Cold"):

$$N_{\text{COLD}} = kTB$$

$f_{\text{OUT}} = [\text{Total Noise Output} / \text{Noise Power due to the Thermal Noise of the Source Impedance}]$:

$$\begin{aligned} f_{\text{OUT}} &= N_{\text{HOT}} / N_{\text{COLD}} \\ &= kTB G_{\text{FILT}} \{ f_{\text{FILT}} - 1 + G_{\text{PA}} [f_{\text{NS}} + f_{\text{PA}} - 1] \} / kTB \\ &= G_{\text{FILT}} \{ f_{\text{FILT}} - 1 + G_{\text{PA}} [f_{\text{NS}} + f_{\text{PA}} - 1] \}. \end{aligned}$$

We can now define the ENR at the THA input as:

$$\text{enr}_{\text{OUT}} = (f_{\text{OUT}} - 1) = \{ G_{\text{FILT}} [f_{\text{FILT}} - 1 + G_{\text{PA}} (f_{\text{NS}} + f_{\text{PA}} - 1)] - 1 \}. \quad (8)$$

Now let's calculate a few fixed quantities:

$$\begin{aligned} \text{ENR}_{\text{NS}}(\text{dB}) &= 13.13 \text{ dB @ } 4 \text{ GHz} \Rightarrow \text{enr}_{\text{NS}} = 20.55891 \Rightarrow f_{\text{NS}} = (\text{enr}_{\text{NS}} + 1) = 21.55891 \\ F_{\text{PA}}(\text{dB}) &= 4.5 \text{ dB @ } 2 \text{ GHz} \Rightarrow \approx 5.5 \text{ dB @ } 4 \text{ GHz} \Rightarrow f_{\text{PA}} \approx 3.54813 \\ G_{\text{PA}}(\text{dB}) &= 14.3 \text{ dB} \Rightarrow G_{\text{PA}} = 26.91535 \\ G_{\text{FILT}}(\text{dB}) &= -0.83 \text{ dB} \Rightarrow G_{\text{FILT}} = 0.82604 \\ f_{\text{FILT}} &= 1/G_{\text{FILT}} = 1/0.82604 = 1.21060 \end{aligned}$$

The ENR of the amplified and filtered noise source is calculated from equation (8) as

$$\begin{aligned} \text{enr}_{\text{OUT}} &= \{ 0.82604[1.21060 - 1 + 26.91535(21.55891 + 3.54813 - 1)] - 1 \} \\ &= \{ 0.82604[0.21060 + 26.91535(24.10704)] - 1 \} = 535.14954 \Rightarrow \text{ENR}_{\text{OUT}}(\text{dB}) = 27.28475 \text{ dB}. \end{aligned}$$

The Y-factor is measured as the ratio of the "hot" and "cold" output noise power:

THA, Post-AMP, & SA Test	Output (dBm)
Noise Source ON	-21.96
Input Terminated (NS OFF)	-23.01
SA Noise Floor	-73.40

$$Y(\text{dB}) = [\text{Non}/\text{Noff}] = [(-21.96\text{dB})/(-23.01\text{dB})] = 1.05 \text{ dB} ; Y = 1.27350.$$

Now we apply equation (7) to calculate the noise figure of the THA, the post-amplifier, and the spectrum analyzer:

$$\begin{aligned} f_{\text{THA, PAMP \& SA}} &= [\text{enr}_{\text{BPFoutput}} / (Y-1)] = [535.14954 / (1.27350-1)] = 1,956.67108, \\ \text{NF}_{\text{THA, Post-AMP, \& SA}}(\text{dB}) &= 10\text{Log}(f) = 32.91518 \text{ dB} \end{aligned}$$

Output Amps, & SA Test	Output (dBm)
Noise Source	-35.53
Input Terminated	-47.67
SA Noise Floor	-88.22

Using the same Y-factor technique, we calculate the noise figure of the post-amplifier and spectrum analyzer as

$$\text{NF}_{\text{Post-AMP, \& SA}}(\text{dB}) = 1.26378 \text{ dB}.$$

The conversion gain of the THA was measured as

$$G_{\text{THA}} (\text{dB}) = -3.74 \text{ dB} \Rightarrow G_{\text{THA}} = 0.47486.$$

We can now calculate the THA noise figure by solving the standard cascaded noise figure equation for f_{THA} :

$$f_{\text{THA}} = f_{\text{THA,Post-AMP, \& SA}} - [(f_{\text{Post-AMP, \& SA}} - 1)/G_{\text{THA}}]. \quad (9)$$

The noise figure of the THA, including the hybrid couplers, is

$$f_{\text{THA}} = 1,956.67108 - [(1.3376-1)/0.47486] = 1,955.96013 ,$$

or in dB:

$$\text{NF}_{\text{THA}}(\text{dB}) = 10\text{Log}(f_{\text{THA}}) = 32.91360 \text{ dB}$$

The insertion loss of the output coupler has a negligible impact on the THA noise figure. However, accounting for the insertion loss of the input hybrid coupler (~ 0.6 dB), we come up with a slightly better estimate for the THA noise figure:

$$\mathbf{\underline{\text{NF}_{\text{THA}} = 32.3 \text{ dB}}}$$

Another, independent noise figure measurement was made. The noise source ENR was increased to increase the Y-factor. A small Y-factor can lead to an erroneous measurement of noise figure. The result was essentially the same.

We note that this noise figure is relatively large. As will be seen in section 4.2.6, the discrete-time measured noise figure is considerably lower. Since we question the validity of the continuous-time noise figure measurement, we will accept the noise figure result given in section 4.2.6.

4.2 Discrete-Time Measurements

In this section, we discuss the discrete-time characterization of the THA. The DRX (Digital Receiver) demo board was used as a sampler and data acquisition front end for all of the discrete-time measurements. The instrument control and DRX demo board data acquisition and analysis was all performed using Matlab [8] scripts, which are listed in the reference section.

4.2.1 The DRX Demo Board Acquisition System

The block diagram of the DRX demo board is shown in Figure 16.

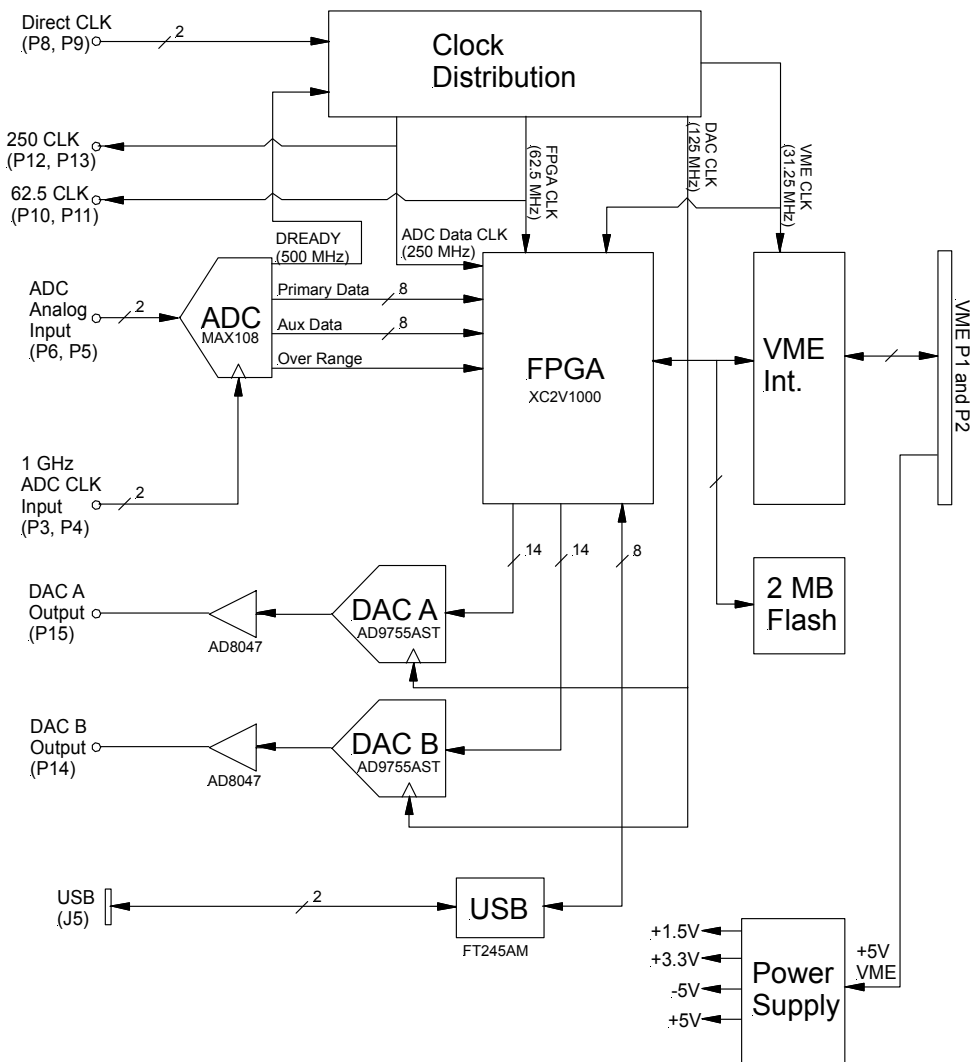


Figure 16: The DRX demo board.

The primary components utilized in the discrete-time measurements are the ADC (Maxim MAX108) operating nominally at 1 GHz, the FPGA (Xilinx XC2V1000), and the VME interface. For each ADC vector acquisition, data is stored in RAM located in the FPGA, then transferred to a Motorola 2307 processor via the VME interface. From there, the data is accumulated (if necessary), then transferred to a PC running Matlab via an ethernet link.

4.2.2 Basic Test Setup

For all discrete-time THA measurements, we used the general test setup shown in Figure 17.

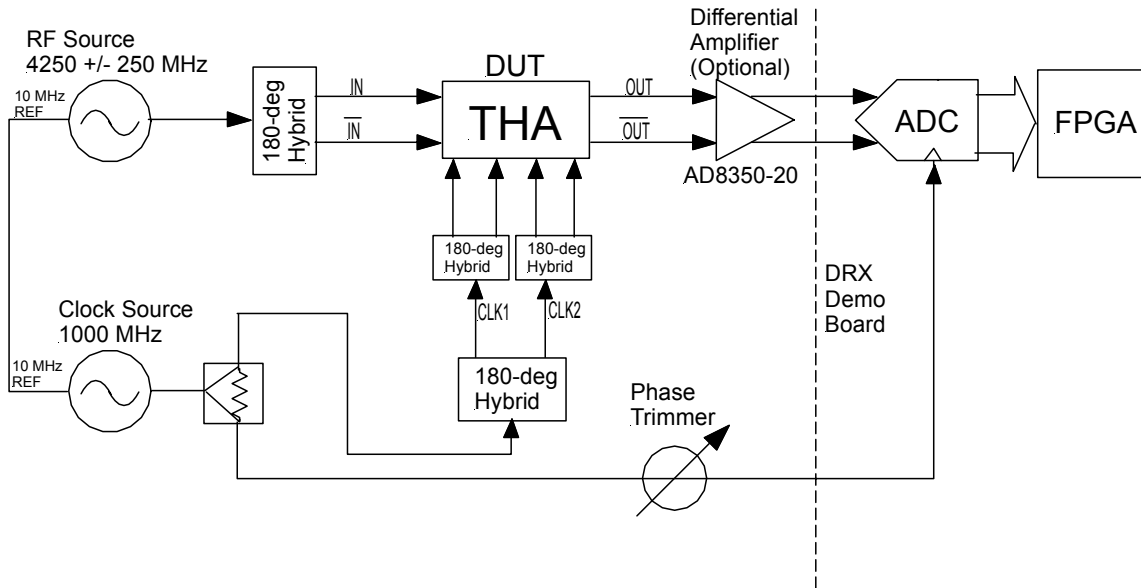


Figure 17: Basic test setup for testing the THA with the MAX108 ADC located on the DRX Demo Board.

All tests are performed using hybrid couplers on the RF and clock inputs for differential operation of the THA. The differential output is either fed directly into the ADC, or pre-amplified using an Analog Devices AD8350-20 differential amplifier.

Both the THA and the ADC are driven by a common clock operating nominally at 1 GHz. A phase trimmer is provided on the ADC clock path to assure that the ADC sample interval falls within the hold interval of the THA. The phase trimmer (Narda model 3752) provides 0 to 180° of relative phase shift at 1 GHz. It was found that no difference in THA and ADC performance was observed over a very wide operating window of approximately $\pm 60^\circ$ centered at mid-scale (90°). This wide phase window was observed when measuring both noise output (section 4.2.6) and intermodulation level (section 4.2.3). For all discrete-time measurements, the phase trimmer was kept roughly in the middle of this window.

4.2.3 Linearity

The ADC acquisition board (DRX demo board) was used to measure the -1 dB compression output power (P_{1dB}) and the output two-tone, third-order intercept (TOI) of the RTH010 THA. The basic test setup is shown in Figure 18.

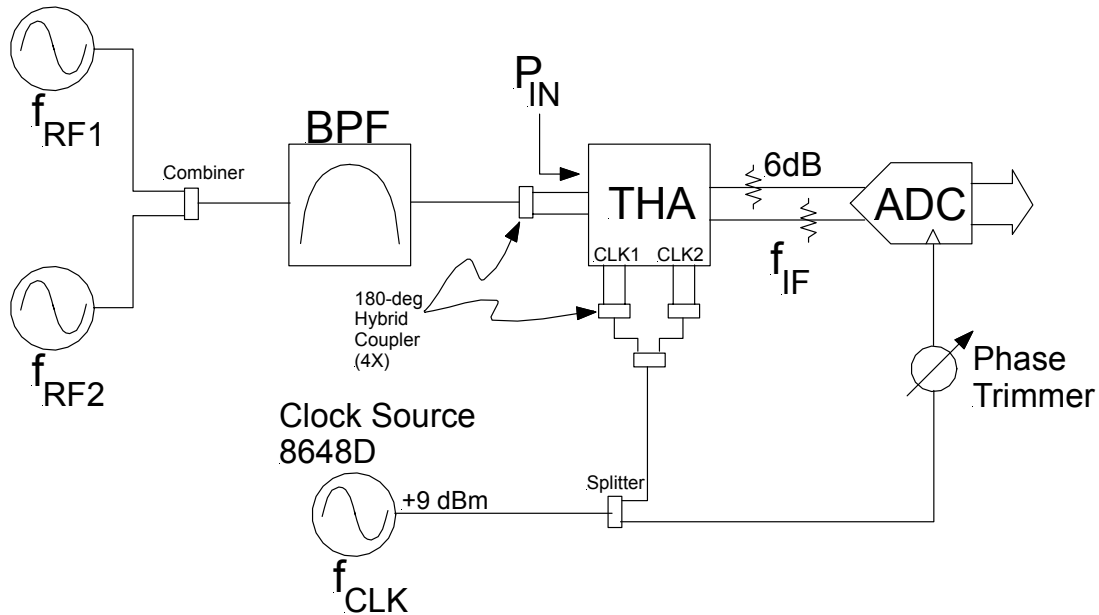


Figure 18: Simplified block diagram of the test setup for measuring the THA linearity.

For the TOI measurement, we used the following parameters:

$$f_{RF1} = 3.8440063 \text{ GHz,}$$

$$f_{RF2} = 3.8538940 \text{ GHz,}$$

$$f_{CLK} = 900 \text{ MHz,}$$

$$f_{IF1} = 244.0063 \text{ MHz,}$$

$$f_{IF2} = 253.8940 \text{ MHz,}$$

THA input hybrid coupler loss = 0.31 dB, and

THA output loss (from THA to ADC on Demo board) = 0.46 dB (no 6 dB pads).

A representative plot of the ADC output spectrum is shown in Figure 19.

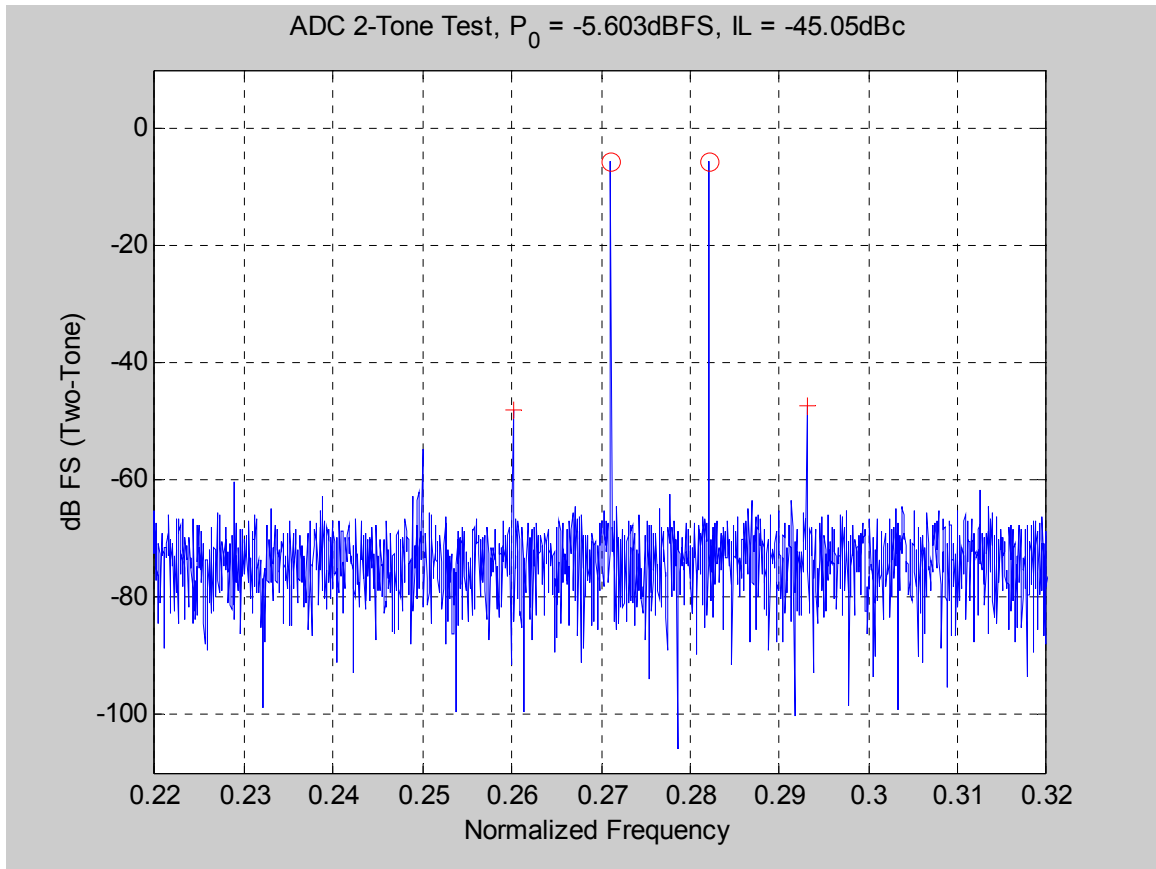


Figure 19: PSD plot showing intermodulation tones.

For the example shown in Figure 19, the intermodulation level $I_3 = -45.1$ dBc. The total output power in both fundamental tones is 5.6 dB below that power which would saturate the ADC. Since the total two-tone power required to saturate the ADC is known (-8 dBm), we can calculate the total output power based on the output power referenced to ADC full scale (dB FS).

Two-tone linearity measurements for the ADC show that at slightly below saturation, the ADC exhibits intermodulation levels of < -60 dBc. This basically means that we can neglect the intermodulation contribution of the ADC as long as the ADC input power < 0 dB FS.

By sweeping the input power, we can plot both the fundamental (P_0) and third-order intermodulation power (P_3) for both tones in dBm. This is shown in **Figure 20**.

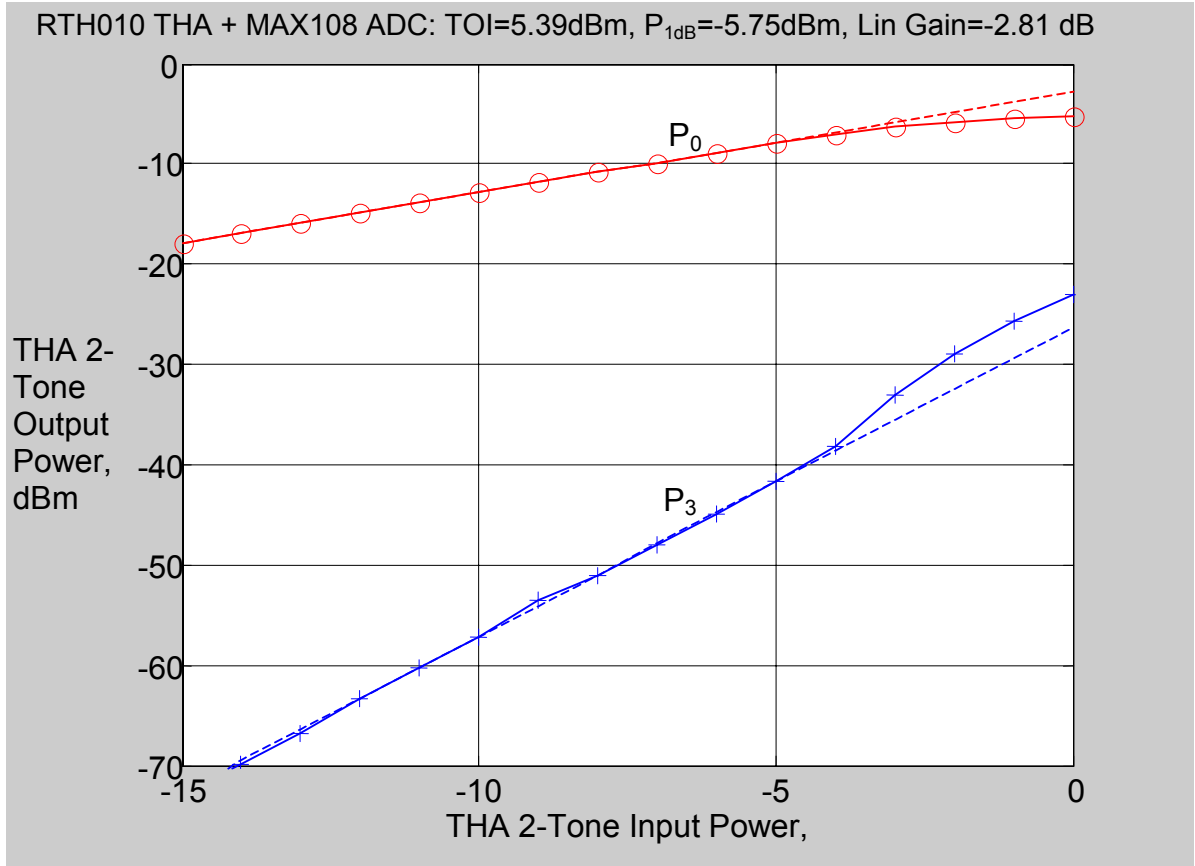


Figure 20: Swept two-tone measurement for the THA and the ADC.

Dashed lines for both the fundamental (P_0) and third-order (P_3) powers are linear fits to the data at input powers which are ≤ -5 dBm. By extrapolating the linear estimates to their intersection, we can calculate the TOI. By convention, we define TOI as

$$TOI(dBm) = P_{0_1T}(dBm) - \frac{I_3(dBc)}{2}, \quad (10)$$

where,

$$I_3(dBc) = P_3(dBm) - P_0(dBm), \quad (11)$$

and,

$$P_{0_1T}(dBm) = P_0(dBm) - 3. \quad (12)$$

In other words, the convention for TOI is based on the single tone output power (P_{0_1T}). Combining equations (11) and (12) into (10) yields

$$TOI(dBm) = \frac{3P_0(dBm) - P_3(dBm)}{2} - 3, \quad (13)$$

where P_0 and P_3 are the total two-tone powers for the fundamental and the third-order intermodulation product respectively in dBm.

For the measurement shown in **Figure 20**, we calculated **TOI = +5.4 dBm**.

The -1 dB output compression point is also calculated as $P_{1dB} = -5.8$ dBm. However, this is based on total two-tone output power. Standard convention is that this be based on a single tone source.

For the single-tone -1 dB compression measurement, we inserted 6 dB fixed attenuators between the THA and the ADC. This ensures that the saturation of the system is not influenced by ADC compression. Figure 21 shows the results of this measurement.

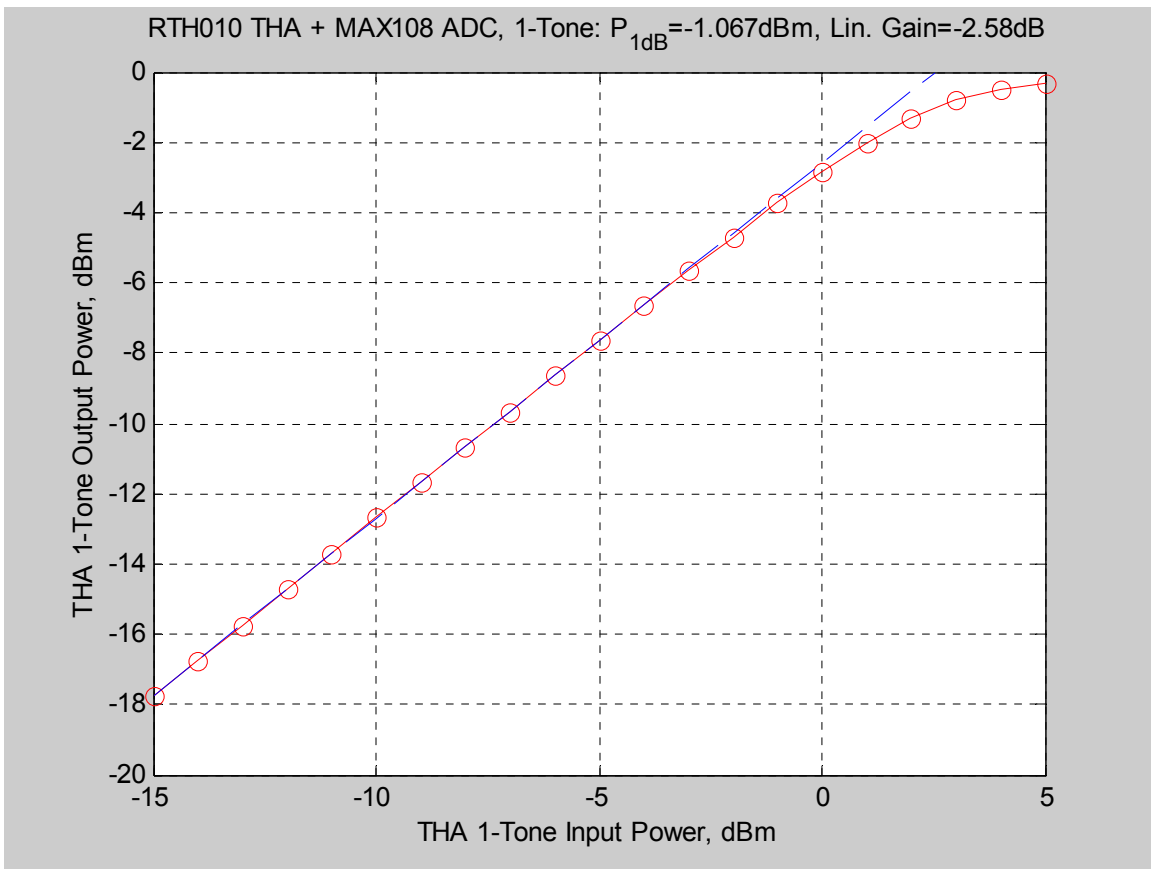


Figure 21: Single tone measurement of the -1 dB output compression point of the THA.

The measured value for the single-tone -1 dB output compression of the THA is **$P_{1dB} = -1.1$ dBm**.

The linear gain of the THA was measured for both the 2-tone and the single-tone cases. The nominal gain from both measurements is approximately -2.7 dB.

It should be noted that the discrete-time measurements for 1 dB compression, TOI, and gain apply to the RTH010 itself. In other words, the loss of the input hybrid coupler is accounted for in each measurement.

4.2.4 Analog Bandwidth

For this measurement, we sweep the RF input into the THA over a broad bandwidth, and measure the insertion loss of the THA vs. frequency. The setup is similar to that shown in Figure 17 with a 1 GHz THA and ADC clock frequency. The THA input hybrid coupler is a Narda model 4346 2-18 GHz hybrid coupler. The coupler has < 0.5 dB peak insertion loss variation over the measured 2 to 10 GHz band, so was considered negligible in the measurement. The results of the wide-band sweep are shown in Figure 22.

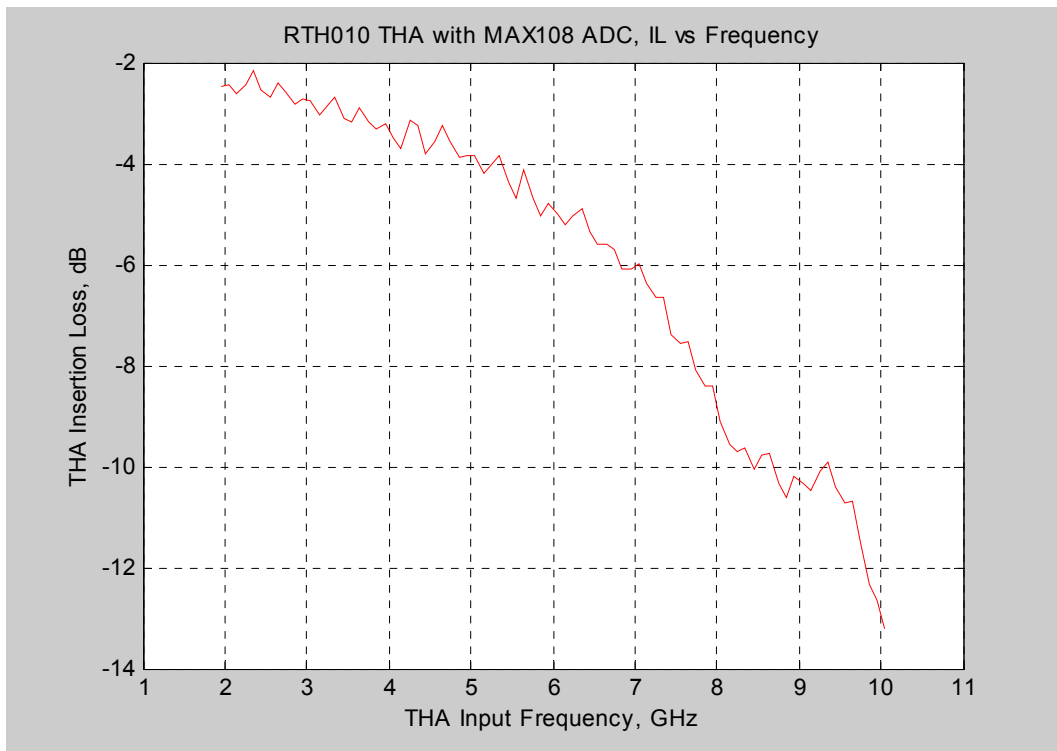


Figure 22: Insertion loss vs. frequency for the RTH010 THA with the MAX108 ADC.

We observe little amplitude roll-off at 4 GHz. However, above 6 or 7 GHz, the insertion loss increases rapidly. It is anticipated that the increase in insertion loss, with the expected decrease in dynamic range performance, would not work well for SAR direct IF sampling applications above 6 GHz, or so.

4.2.5 Signal-to-Noise Ratio and Spurious-Free Dynamic-Range

The Signal-to-Noise Ratio (SNR) and Spurious-Free Dynamic Range (SFDR) of the THA and the ADC (MAX108, 1 GS/s, 8-bit) were measured as a function of RF source frequency. The RF frequency was selected based on the requirements of the THA to facilitate the undersampling of the 4 GHz IF of our existing SAR.

The RTH010 THA evaluation board differential output was connected to the ADC inputs on the DRX demo board with the 1 GS/s MAX108 ADC. The THA was driven from an RF source with a nominal center frequency of 4000 MHz. A 4000 MHz centered, 380 MHz bandwidth bandpass filter was inserted between the RF source and the THA DUT to ensure that source harmonics do not affect the SNR and SFDR measurements. The simplified diagram of the test setup is shown in Figure 23.

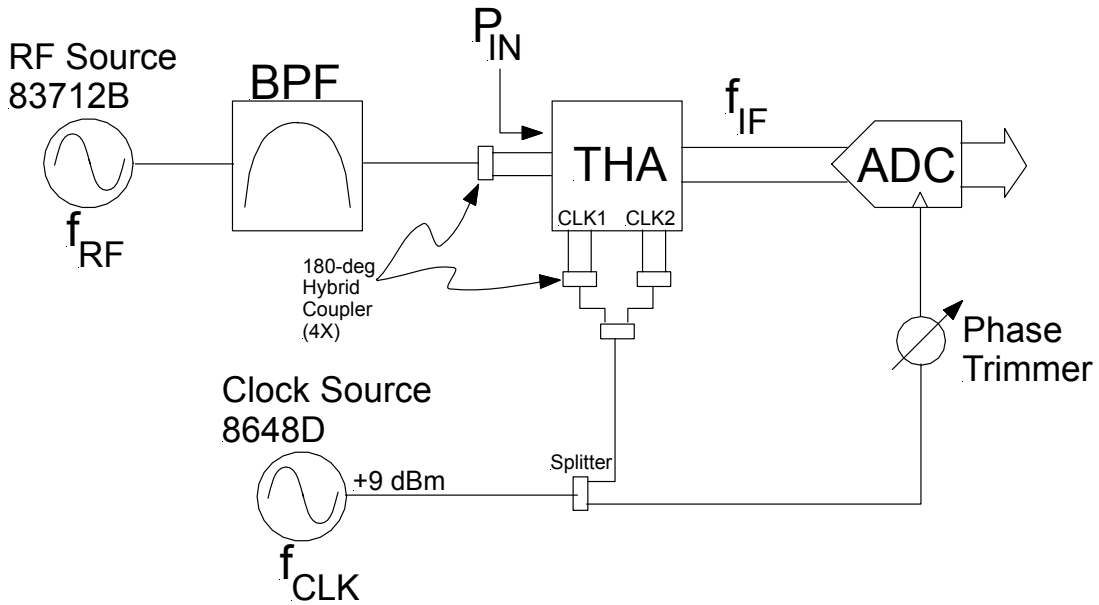


Figure 23: Test setup for measuring the SNR and SFDR for the THA with the 1 GS/s ADC.

The source and clock frequencies were selected based on a desired RF center frequency of $f_{RF} = 4000$ MHz and an IF center frequency of $f_{IF} = 250$ MHz. For given RF and IF frequencies, the clock frequency f_{CLK} must satisfy

$$f_{CLK} = \frac{f_{RF} \pm f_{IF}}{k}, \quad (14)$$

where k is any positive, non-zero integer. The clock frequency which satisfies our requirements for nominal f_{RF} and f_{IF} which is closest to 1000 MHz was selected as $f_{CLK} = (f_{RF} + f_{IF})/4 = 1062.5$ MHz (i.e., $k = 4$).

The power level into the THA (P_{IN}) is selected based on measurements of the THA third-order intercept (TOI) which yields acceptable third-order intermodulation levels. A P_{IN} level of a single RF tone which is approximately 5 dB below the ADC saturation level (-5 dBFS) is acceptable. This corresponds to $P_{IN} \cong -7$ dBm. The flatness of the THA input power at the IN+ and IN- ports was measured to be -0.4 dB and +0.2 dB deviation from the power at 4 GHz, as measured over a 300 MHz span.

Figure 24 shows an example PSD plot with $f_{RF} \cong 4$ GHz and $P_{IN} = -7$ dBm.

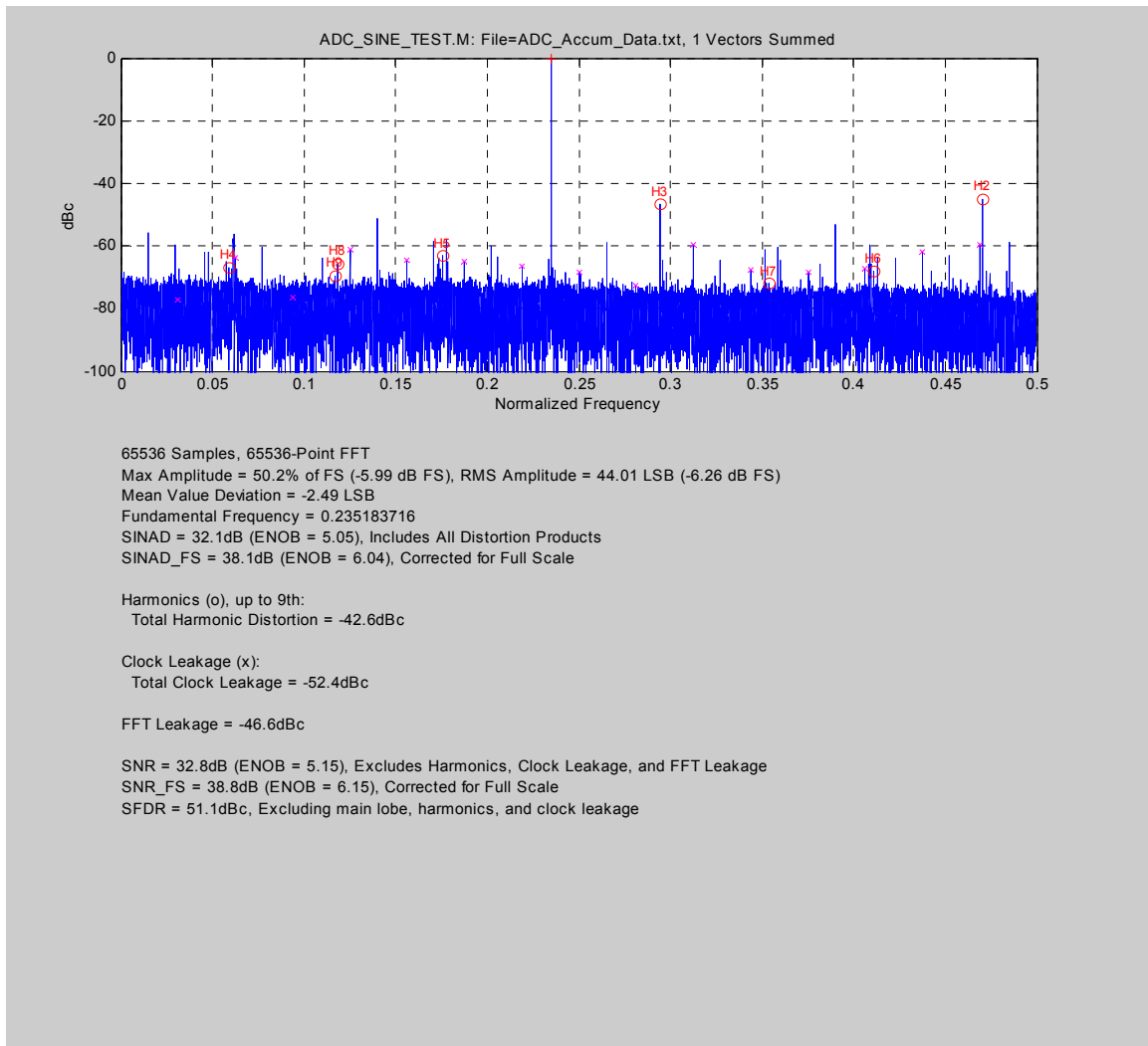


Figure 24: Example PSD plot of THA and ADC with $f_{RF} \cong 4$ GHz and $P_{IN} = -7$ dBm.

When calculating the SNR and SFDR, we want to make sure to exclude those spurious signals of known origin and/or that are due to non-idealities of the test setup. Those terms include source harmonics, ADC board clock leakage, and FFT leakage.

Harmonics of the fundamental, which appears at ~ 250 MHz or at a normalized frequency of $\sim 250/1062.5 = 0.235$, are calculated and marked with an “o”. For this plot, we

calculated the total harmonic distortion (THD) at -42.6 dBc up to the 9th harmonic. Another spurious source is the FPGA (field programmable gate array located on the ADC acquisition board) clock leakage which appears at multiples of $f_{CLK}/32$. The clock leakage terms are marked with an “x”, with all clock terms contributing to a -52.4 dBc clock leakage level. Another source of sidelobe energy is the FFT leakage. The source frequency is calculated such that an even number of cycles at IF are sampled over the ADC aperture. However, some small amount of FFT leakage still exists. In this example, the FFT leakage around the main lobe is at a level of -46.6 dBc.

Once the harmonic, clock, and FFT leakage terms are accounted for (i.e. removed), we basically calculate the integrated sidelobe energy as the SNR, and the peak relative sidelobe energy as the SFDR. For the PSD of Figure 24, the SNR = 32.4 dB, and the SFDR = 51.1 dB. We also calculate a modified version of the SNR which accounts for the fact that the signal level is not taking advantage of the full dynamic range of the ADC. In other words, the SNR corrected for ADC full scale (SNR_{FS}) calculates the equivalent SNR of a signal at the ADC full scale level. Since the signal shown in Figure 24 is 6 dB below ADC full scale (-6 dB FS), an ideal amplifier with 6 dB of gain placed between the THA and the ADC would yield an SNR equivalent to SNR_{FS} . In the case of Figure 24, $SNR_{FS} = 38.8$ dB.

The ADC alone obtains SNR_{FS} performance of 47 dB (7.5 effective bits) consistently. With the THA, the SNR is degraded by approximately 8.2 dB, which is equivalent to “losing” 1.4 bits of dynamic range performance. This may present a problem for SAR applications where dynamic range at the ADC is paramount.

The behavior of SNR, SNR_{FS} , SFDR, and -THD as a function of RF frequency is illustrated in Figure 25. The Signal to Harmonic Ratio (SHR) in dB is equal to the negative of the THD in dB (i.e. $SHR(dB) = -THD(dB)$).

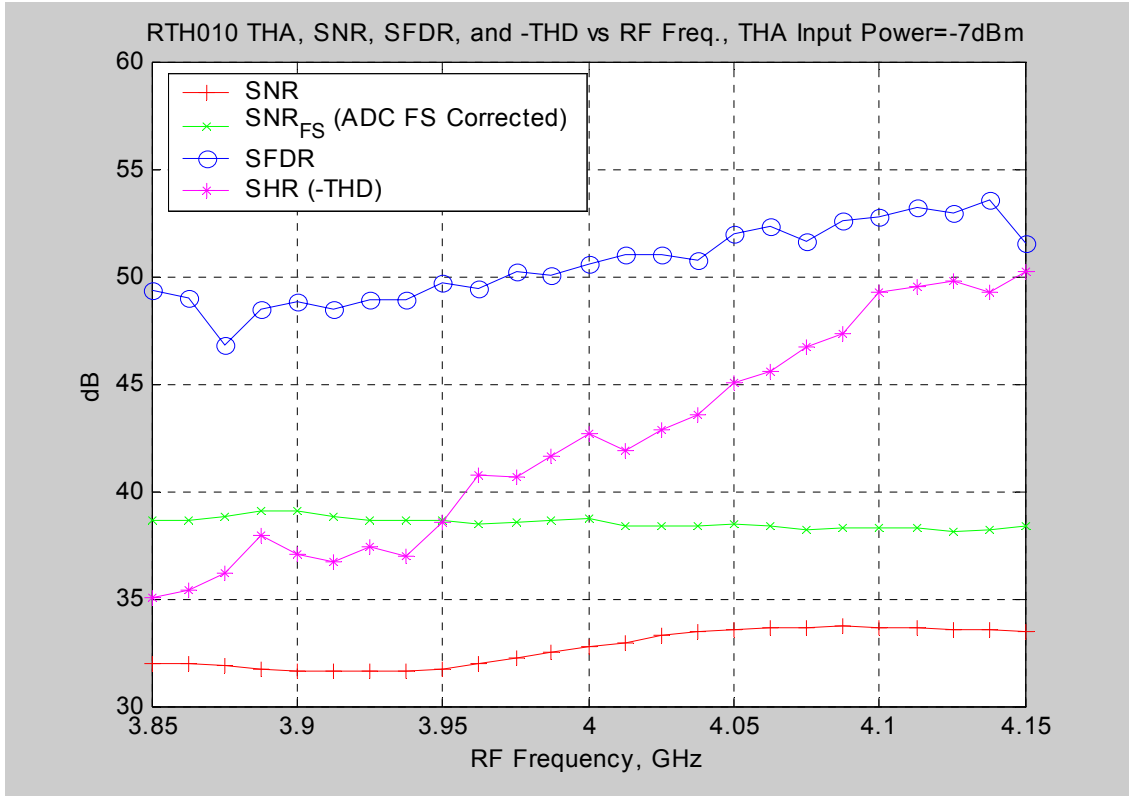


Figure 25: SNR, SNR_{FS}, and SFDR vs. RF frequency.

With the exception of THD, the parameters do not change dramatically vs. frequency.

By sweeping the RF input power level, then measuring the average values for SNR, SNR_{FS}, SFDR, and THD over the swept bandwidth, we can plot each parameter as a function of RF input power. Figure 26 shows the results of this measurement.

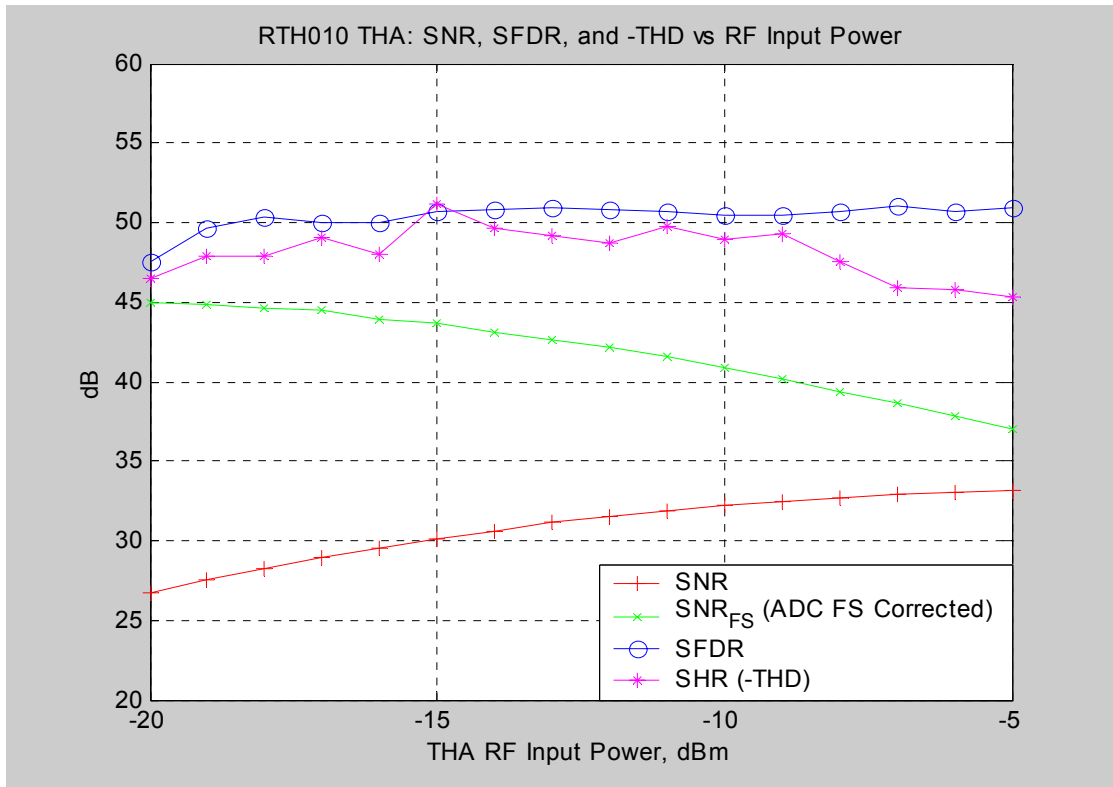


Figure 26: SNR, SNR_{FS}, SFDR, and -THD vs. RF input power level.

Note that the full-scale corrected SNR (SNR_{FS}) degrades as the input power level is increased. However, the SFDR is constant. This suggests that the spurious are first-order with respect to the signal. Thus, their power levels are directly proportional to the signal power level. We also observe that the THD is also relatively constant. This is a somewhat surprising result.

Based on the measurements made above, we can make a few summary comments.

- The THA generates additional spurious output which degrades the “effective” ADC dynamic range by approximately 8.2 dB. This may not be acceptable for many SAR applications where dynamic range is paramount.
- The spurious output level is not a strong function of frequency over a 300 MHz bandwidth centered at 4000 MHz.
- The additional spurs are proportional to the signal level. Therefore, their relative power level to the signal (dBc) does not change vs. THA input power. This is also not good.

In general, any high-performance, high-dynamic range radar system will need to carefully consider the SNR and SFDR performance of the THA. Results of the above measurements show that the SNR and SFDR performance of the RTH010 destined for SAR receiver applications which employ stretch (deramp) processing is marginal at best.

4.2.6 Noise Figure

There is some doubt as to the validity of using an instrument such as a spectrum analyzer to measure the Y-factor for determination of the noise figure of the THA. Since the spectrum analyzer integrates the total noise power over the entire track and hold cycle of the THA, additional noise may be present which is not representative of the noise present when the ADC samples the signal.

In this measurement, the DRX (Digital Receiver) demo board was used to sample, quantize, and acquire the data during the hold interval of the THA. A clock frequency f_{CLK} of 1062.5 MHz was selected for an RF center frequency of 4 GHz, and an IF (ADC input) center frequency of 250 MHz nominal. A simplified block diagram of the test setup is shown in Figure 27.

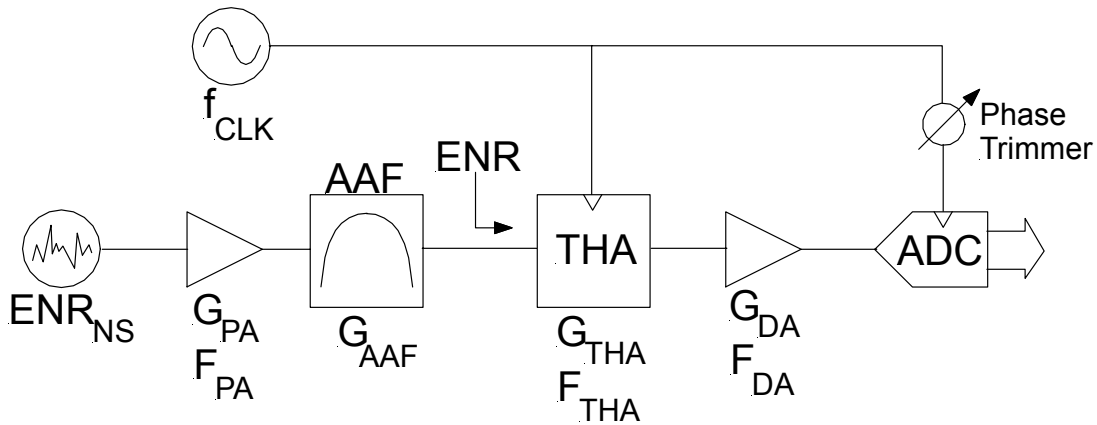


Figure 27: Block diagram of noise figure test setup.

The noise source consists of an HP346B with $ENR_{NS} = 14.7$ dB at 4 GHz. Due to the relatively high expected noise figure of the THA, a preamp (Miteq AMF-4B-2040-25) with a gain $G_{PA} = 42.4$ dB and a noise figure $F_{PA} = 2.7$ dB at 4 GHz was used to increase the noise level of the overall noise source with an equivalent input noise ratio ENR. An anti-aliasing filter (AAF) with gain $G_{AAF} = -0.6$ dB and a bandwidth of approximately 135 MHz was used to ensure that the noise is only generated in the Nyquist band of interest. The ENR of the HP346B noise source, the preamp, and the AAF can be calculated as:

$$ENR = G_{AAF}[G_{PA}(F_{PA} + ENR_{NS}) - 1]. \quad (15)$$

Plugging in the values above into equation (15) yields

$$ENR = 478.6 = 56.8dB.$$

The DUT is the RTH010 THA with a measured gain $G_{THA} \approx -3.0$ dB and an unknown noise figure F_{THA} .

An Analog Devices AD8350-20 differential amplifier (DA) was added between the THA and the ADC to ensure that adequate noise is always present at the ADC input. This ensures that the ADC output quantization noise is random and statistically independent from the noise at the ADC input. The differential amplifier has a gain $G_{DA} = 20$ dB and a noise figure $F_{DA} = 5.9$ dB at 250 MHz. As we will see in subsequent calculations, the actual value for G_{DA} is not important as long as it is large enough to provide adequate noise into the ADC for the case when the noise source is OFF (i.e., the input is terminated into 50 ohms). The DA noise figure F_{DA} is accounted for in the calculations, however, it has little impact on the end result.

From the diagram of Figure 27, we can express the noise figure of the THA as

$$F_{THA} = F_T - \frac{F_{DA} - 1}{G_{THA}}, \quad (16)$$

where F_T is the overall noise figure of the THA and the differential amplifier (DA).

To acquire F_T , we use the Y-factor method. The Y-factor is the ratio of the ADC output noise power (or variance σ^2) with the noise source (HP346B + preamp) ON, to the power (or variance) with the noise source OFF. In terms of variance at the ADC output, we can write

$$Y = \frac{\sigma_{ADC_ON}^2}{\sigma_{ADC_OFF}^2}. \quad (17)$$

Equation (17) is valid if the quantization variance is much smaller than the variance due to noise at the input of the ADC. This requirement is satisfied when the DA is inserted between the THA and the ADC. Also, it is desirable to calculate the noise variance σ^2 of the ADC output from the discrete-Fourier transformed (DFT) data over a subset of the Nyquist bandwidth. This ensures that only the noise in the band of interest as dictated by the AAF is measured.

F_T is determined from Y as

$$F_T = \frac{ENR}{Y - 1}. \quad (18)$$

The basic procedure is to determine Y based on equation (17). The ON and OFF variances are calculated as

$$\sigma_{ADC}^2 = \sum_{n=n1}^{n2} \left| DFT(x_n - \overline{x_n}) \right|^2, \quad (19)$$

where x_n are the raw ADC output samples, $\overline{x_n}$ is the mean of x_n , $DFT()$ denotes the discrete Fourier transform, and $n1$ and $n2$ denote the data indices corresponding to the minimum and maximum normalized frequencies $\omega1$ and $\omega2$ over which we want to calculate the noise variance. For the purposes of this experiment, $\omega1 = 0.2$ and $\omega2 = 0.3$, as normalized to f_{CLK} .

Figure 28 shows a plot of the ADC output power spectral density (PSD) vs. normalized frequency with the noise source ON.

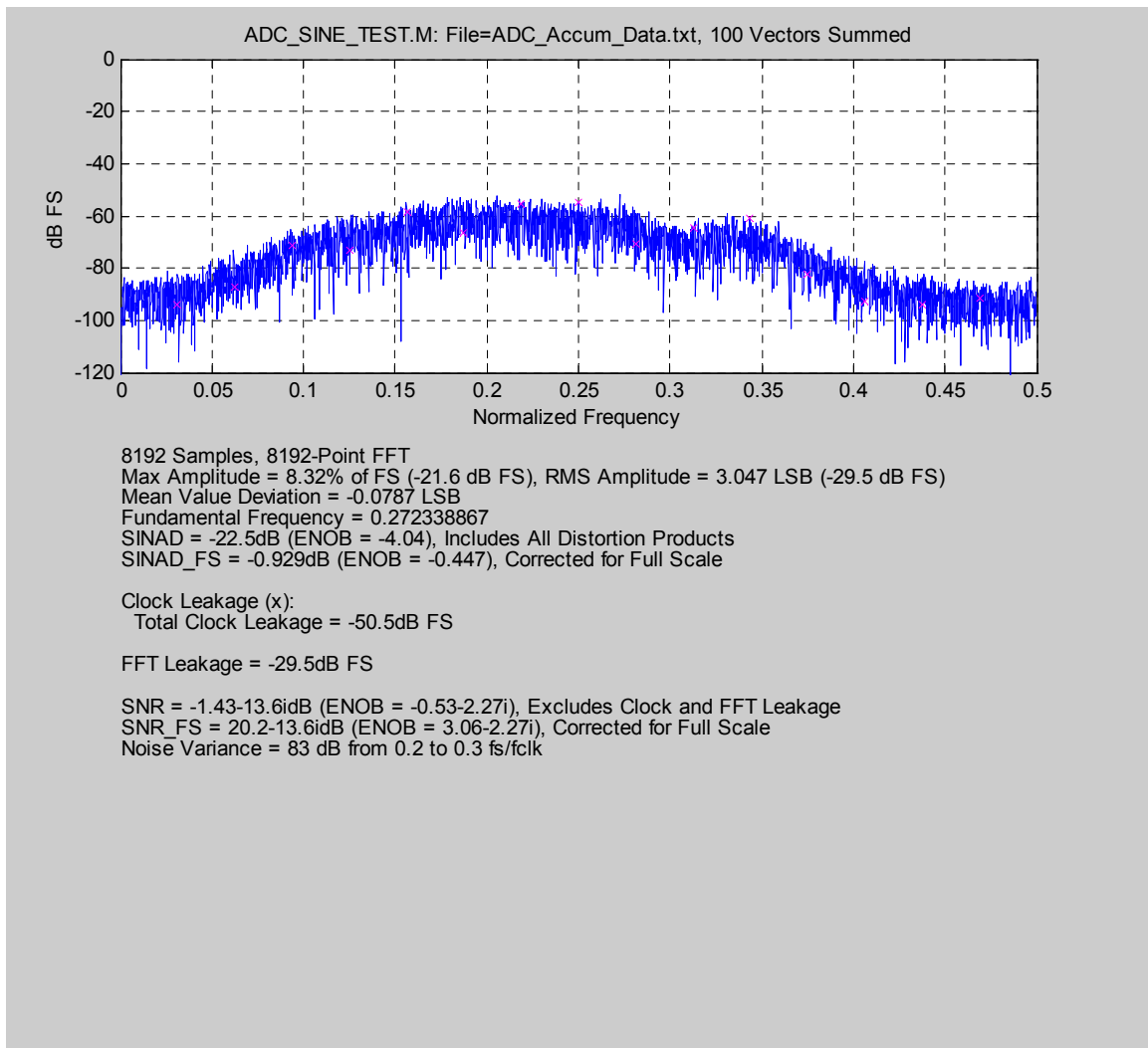


Figure 28: ADC output noise PSD plot with noise source ON.

Here, we measured the noise variance of the 8-bit, zero-mean integer data at the ADC output from $\omega = 0.2$ to 0.3 as

$$\sigma_{ADC_ON}^2 = 199.5 = 83dB.$$

Multiple vectors are summed (100 in this case) to improve measurement-to-measurement consistency, and to remove the FPGA clock leakage spurs through $0/\pi$ modulation.

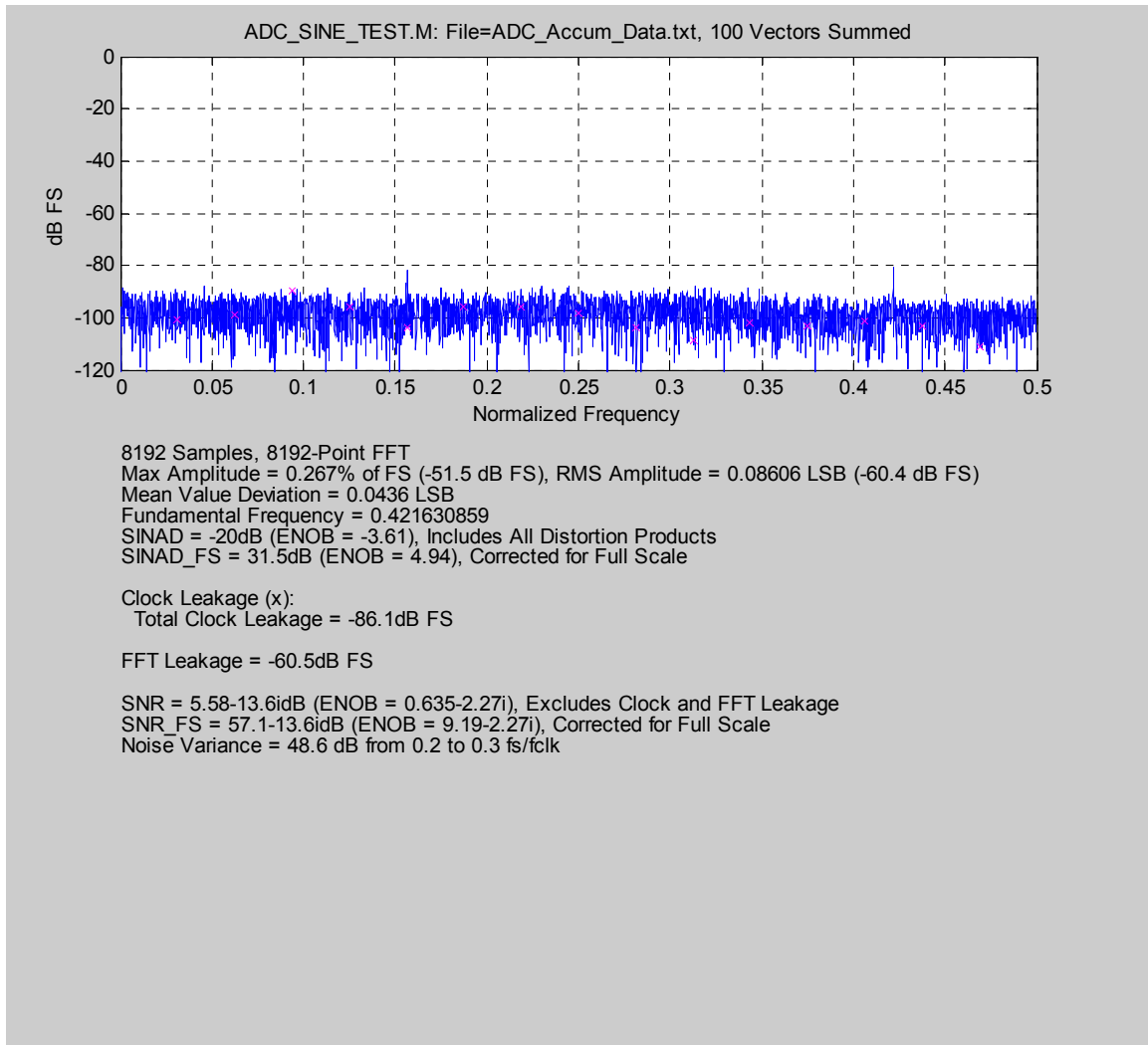


Figure 29: ADC output noise PSD plot with noise source OFF.

Figure 29 shows the PSD with the noise source OFF. For the noise OFF case, we measured the noise variance from $\omega = 0.2$ to 0.3 as

$$\sigma_{ADC_OFF}^2 = 72.4 = 48.6dB .$$

From equation (17), the Y-factor is calculated as

$$Y = 2754 = 34.4dB .$$

From equation (18), we calculate F_T as

$$F_T = 173.8 = 22.4dB .$$

Equation (16) gives us the desired THA noise figure:

$$F_{THA} = 166.0 = 22.2dB .$$

Since both F_{THA} and G_{THA} values include a 0.3 dB hybrid coupler loss, we can adjust F_{THA} to give our best estimate for the THA noise figure:

$$\underline{F_{THA} = 21.9dB .}$$

Note that this is considerably lower than the ~32 dB measured using continuous time measurement. An optimist would choose the lower value. We choose the lower value based on the argument that using continuous measurement for THA noise figure is simply not valid. This is due to the presents of additional integrated noise in the continuous-time measurement vs. the total integrated noise over the sampler acquisition interval as measured using the discrete-time technique.

5 Analysis of THA Performance vs SAR Requirements

In this section, we take a quantitative look at the THA measurements and their potential impact to the performance of the Sandia National Laboratories SAR research platform.

5.1 Phase Noise

The introduction of phase noise or timing jitter due to the THA can degrade the SNR performance of the SAR in the Doppler domain. The basic question is, “how much phase noise at the THA is tolerable in our SAR IF sampling application?” The answer is, “a lot more than the measured phase noise performance of the THA.”

Armin Doerry [9] has formulated an upper limit on the total RMS timing jitter for an ADC in a SAR application. We can use this same limit for considering the phase noise contribution of the THA:

$$\Delta t_{RMS} \leq \frac{10^{\frac{MNR}{20}}}{2\pi f_{IF_MAX}}, \quad (20)$$

where, MNR refers to the allowable multiplicative-noise ratio contribution of the timing jitter (we can think of it in this context as directly effecting the SNR), and f_{IF_MAX} is the maximum ADC input frequency. For our application, the THA phase noise contribution is negligible if $MNR < -50$ dB for $f_{IF_MAX} = 4125$ MHz. This results in a requirement that $\Delta t_{RMS} \leq 0.217$ psec. For the RTH010, we measured a mere 0.0472° RMS total phase noise, which equates to an RMS timing jitter of 0.0318 psec at 4125 MHz. Obviously, THA phase noise is not a problem!

Its interesting to note, assuming RMS phase noise remains constant vs. frequency, that the low phase noise of the RTH010 makes it possible to direct sample at Ku-band frequencies! The analog bandwidth and linearity performance of the RTH010 at Ku-band, however, will prevent this from becoming reality.

5.2 Dynamic Range: Linearity vs. Noise Figure

We can model the radar with a THA as an analog RF subsystem with gain G_{RX} and noise figure F_{RX} , and IF bandwidth of B_{RX} . The THA has gain G_{THA} and noise figure F_{THA} . Since linearity measurements of the THA suggest that a differential amp will be needed between the THA and the ADC, we will assume that this device has a gain G_{DA} and noise figure F_{DA} . The model for this system is shown in Figure 30.

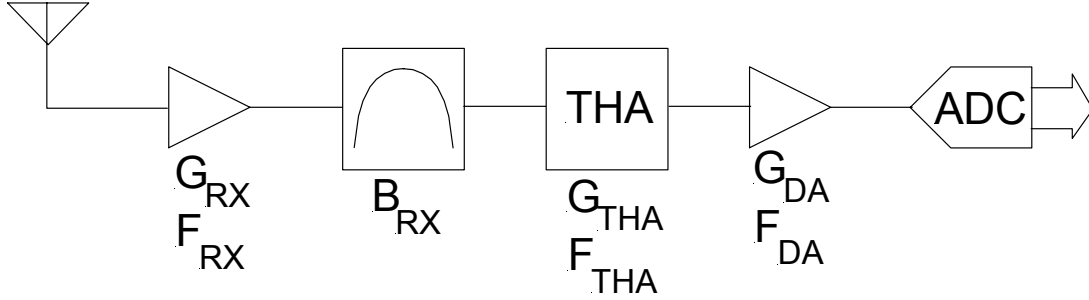


Figure 30: Model of radar RF system with a THA and a preamp.

Applying cascade calculations, we can write the equations for the total gain G_T and the overall system noise figure F_T :

$$G_T = G_{RX} G_{THA} G_{DA}, \quad (21)$$

and

$$F_T = F_{RX} + \frac{F_{THA} - 1}{G_{RX}} + \frac{F_{DA} - 1}{G_{RX} G_{THA}}. \quad (22)$$

The basic question to be answered is, “What is the effect of the THA noise figure F_{THA} on the overall system noise figure F_T ?” To answer this, we need to write F_T as a function of F_{THA} as is given in equation (22). Next, we need to determine values or equations for the other variables.

For the differential amp (DA), we used the differential in/out AD8350 [6] as an ADC preamp. This device has a 5.9 dB noise figure ($F_{DA} = 3.89$) and a +28 dBm Third-Order Intercept (TOI) as reference to its output, meaning we can basically neglect the effect of the preamp on system linearity.

As for the preamp gain, we need to figure this out based on the ADC saturation power and the THA TOI (lab measured $TOI_{THA} \approx +5$ dBm). We desire to place a limit on the minimum tolerable third order intermodulation level I_3 when the ADC is saturated. Reasonably good performance is obtained with $I_3 = -40$ dBc maximum. For two sinusoidal tones at the THA output, each with a power of $P_{THA_OUT_1T}$ in dBm, we can write:

$$P_{THA_OUT_1T} (dBm) = TOI_{THA} \sqrt{I_3} = TOI_{THA} (dBm) + \frac{I_3 (dBc)}{2}. \quad (23)$$

Given the measured value of $TOI_{THA} = +5$ dBm and the desired minimum value of $I_3 = -40$ dBc, we get $P_{THA_OUT_1T} = -15$ dBm per tone which is a total power of $P_{THA_OUT_2T} = -12$ dBm for both tones.

As for the ADC (MAX108) saturation power, the total differential, single-tone input power P_{ADC_1T} which saturates the ADC is

$$P_{ADC_1T} = \frac{V_{ADC_PP}^2}{8Z_{ADC}}, \quad (24)$$

where V_{ADC_PP} is the ADC saturated input differential peak-to-peak voltage ($V_{ADC_PP} = 0.5$ V) and Z_{ADC} is the ADC differential input impedance ($Z_{ADC} = 100\Omega$). Using equation (24), we get the total single-tone saturation power at the ADC input $P_{ADC_1T} = -5.05$ dBm. The total saturation power for two-tones at the ADC input is simply half that of the single tone power or $P_{ADC_2T} = -8.06$ dBm. The required preamp gain is the ratio of ADC input saturation power to the THA output power:

$$G_{DA} = \frac{P_{ADC_2T}}{P_{THA_OUT_2T}}, \quad (25)$$

or $G_{DA} = 4$ dB. This is a very small gain, which suggests that we may not need to sacrifice too much by way of intermodulation performance by deleting the preamp altogether. The intermodulation level we would achieve without the preamp is obtained by setting P_{THA_OUT} in equation (23) to -11.07 dBm (per tone power which saturates the ADC) and solving for I_3 which gives $I_3 = -32.1$ dBc. For some radar applications, this may be acceptable. For Sandia-built SARs, this is marginal.

Discrete-time measurements of the THA with and ADC put the gain at $G_{THA} \cong -3$ dB and the noise figure $F_{THA} \cong 22$ dB. This is based on an input frequency of ~ 4 GHz, an output frequency of ~ 250 MHz, and a nominal clock frequency of ~ 1 GHz.

As for the noise figure of the radar receiver (F_{RX}), this varies considerably from application to application. Typical values range from 4 dB to 6 dB. It will be seen in the analysis to follow, that since we can write an expression for the receiver NF degradation, the absolute value of F_{RX} need not be known.

The gain of the radar receiver (G_{RX}) is typically set to achieve adequate noise power at the ADC input. Billy Brock's analysis [4] has shown that an RMS noise level of approximately 1 LSB (Least-Significant Bit) at the ADC input provides adequate noise dither while maximizing the radar dynamic range performance.

Let's begin by defining the total noise power N_{ADC} at the ADC input based on the total system gain and noise figure:

$$N_{ADC} = kTB_{RX}G_TF_T, \quad (26)$$

where k is Boltzman's constant (1.38×10^{-23} Wsec/K) and T is the temperature in $^{\circ}K$ (we will use $25^{\circ}C$ or $298^{\circ}K$).

We stated above that we desire to set the RMS noise voltage into the ADC to 1 LSB RMS. The total noise power into the ADC under this condition is

$$N_{ADC_1LSB} = \frac{V_{ADC_PP}^2}{2^{2n_{ADC}} Z_{ADC}}, \quad (27)$$

where n_{ADC} is the effective number of ADC bits ($n_{ADC} \cong 7.5$ bits for the MAX108). Setting $N_{ADC} = N_{ADC_1LSB}$ and solving for the total receiver gain yields

$$G_T = \frac{V_{ADC_PP}^2}{kTB_{RX} 2^{2n_{ADC}} Z_{ADC} F_T}. \quad (28)$$

Substituting equation (21) into equation (28) and solving for G_{RX} yields

$$G_{RX} = \frac{V_{ADC_PP}^2}{kTB_{RX} 2^{2n_{ADC}} Z_{ADC} G_{THA} G_{DA} F_T}. \quad (29)$$

Equation (29) basically defines the pre-THA gain required to set the proper noise level into the ADC. By substituting equation (29) into equation (22), we get our desired expression for F_T :

$$F_T = \frac{V_{ADC_PP}^2 F_{RX}}{V_{ADC_PP}^2 + [G_{THA}(1 - F_{THA}) - F_{DA} + 1]kTB_{RX} 2^{2n_{ADC}} Z_{ADC} G_{DA}}. \quad (30)$$

Better yet, lets write an expression for the overall noise figure degradation:

$$F_{Degrade} = \frac{F_T}{F_{RX}} = \frac{V_{ADC_PP}^2}{V_{ADC_PP}^2 + [G_{THA}(1 - F_{THA}) - F_{DA} + 1]kTB_{RX} 2^{2n_{ADC}} Z_{ADC} G_{DA}}. \quad (31)$$

Equation (31) defines the degradation to the system noise figure due to the THA noise figure and gain. Plugging in the aforementioned fixed values:

$V_{ADC_PP} = 0.5$ V, (MAX108 ADC, differential input)
 $G_{THA} = 0.5$ (-3 dB),
 $G_{DA} = 2.51$ (4 dB),
 $F_{DA} = 3.89$ (5.9 dB),
 $B_{RX} = 380$ MHz,
 $n_{ADC} = 7.5$, and (MAX108 at 250 MHz input, 1 GS/s)
 $Z_{ADC} = 100\Omega$ (differential),

into equation (31), we can plot the noise figure degradation vs the THA noise figure as shown in Figure 31.

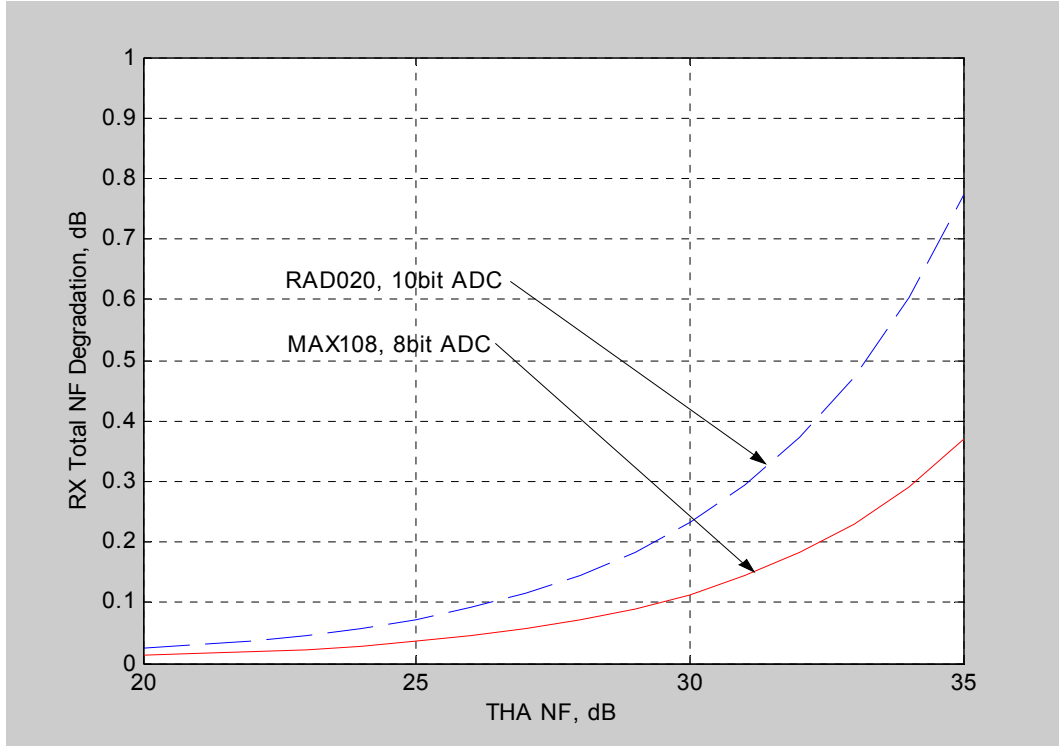


Figure 31: Radar receiver NF degradation vs THA NF.

Since we also have a future interest in the Rockwell RAD020 10-bit ADC [5]¹, we include a NF degradation plot with $n_{ADC} = 9$ effective bits² and $V_{ADC_PP} = 1$ V.

Note that the NF degradation for the receiver using the MAX108 or the RAD020 ADC is < 0.05 dB assuming a THA NF (F_{THA}) of 22 dB. We typically like to see NF degradations < 0.1 dB, so we consider the THA noise figure performance to be acceptable for our SAR applications.

In the effort to maximize the dynamic range of a receiver, it may be desirable to trade-off noise figure for linearity (intermodulation level). Since we have selected the preamp gain G_{DA} such that a desirable maximum intermodulation level I_3 be obtained, let's now make I_3 an independent variable. Substitution of equations (23) and (24) into (25) yields

¹ The RAD020 includes an internal 2-stage 9 GHz bandwidth THA which is assumed to have equivalent performance to the RTH010.

² The preliminary data sheet shows the SNR performance of the RAD020 to be approximately 8.5 effective bits at the Nyquist frequency, assuming a 1 GHz clock. 9 effective bits is an extrapolated estimate for the performance at 250 MHz input.

intermodulation level, which is marginal to unacceptable for some SAR applications.

- With a differential gain stage inserted between the THA and the ADC, we can improve the intermodulation level to -45 dBc (or perhaps lower) with negligible impact on system noise figure.

5.3 SNR Degradation and SFDR

Perhaps the most worrisome performance aspect of the RTH010 for our 4 GHz IF sampling application is the SNR degradation. As discussed in section 4.2.5, the THA at 4 GHz degrades the ADC dynamic range (SNR) performance by 8.2 dB or, stated another way, we effectively “lose” 1.4 bits. Further analysis and measurement of the THA and ADC will need to be performed to better understand the impact of this SNR degradation under specific SAR imaging scenarios.

We consistently identify the ADC as the primary dynamic range limiter in any SAR employing stretch processing. It is for this reason that any degradation to the SNR performance of the sampler will directly impact the overall SAR dynamic range. In other words, we want samplers (THA and ADC combinations) to have as high an SNR as possible.

The SFDR of the THA is approximately 50 dBc. This is acceptable, as we typically require at least 40 dB and prefer 45 dB for most applications.

6 Summary

We summarize the measurements performed on the THA in Table 1. All measurements assume a nominal input frequency of 4 GHz and a nominal clock frequency of 1 GHz.

Table 1: THA Measurements Summary

Parameter	Continuous-Time	Discrete-Time
Insertion loss	3.5 dB	2.6 dB
1 dB Gain Compression Output Power	-2.1 dBm	-1.1 dBm
Output Third-Order Intercept	+5.5 dBm	+5.4 dBm
RMS Phase Noise	0.047°	————
Noise Figure	~ 32 dB	21.9 dB
Spurious-Free Dynamic Range	————	~ 50 dB
Signal-to-Noise Ratio (excluding harmonics) reference to ADC Full-Scale Input	————	~ 39 dB

We note that the linearity measurements (1 dB compression and TOI) agree very well between the continuous and discrete-time measurements. We also note that the high noise figure measurement for the continuous-time case is, most likely, invalid due to the presence of additional noise outside of the hold interval of the THA.

We can summarize the “goodness” of the performance parameters, based on the requirements of our SAR IF sampling application as follows:

- Good (it will work!)
 - Analog Bandwidth
 - Phase Noise
 - Noise Figure
- Acceptable (some room for improvement)
 - Linearity
 - SFDR
- Marginal to Poor (may need design improvement to be acceptable)
 - SNR

This is a very subjective assessment, but it does give a very terse summary, for those readers who want to be spared the details.

Based on the summary above, and our current desires for future direct sampling radar receiver architectures, we can list a few general questions and/or comments which could lead to future tasks.

- How do we improve the SNR performance of the THA? What other performance aspects, if any, do we sacrifice in doing so?
- Can detailed non-linear circuit analysis of the THA lead to a product which better fits our applications?
- A SAR which employs stretch processing has less signal dynamic range at RF than at IF. For some applications, direct RF sampling at X-band or Ku-band may be possible. This needs further measurement and analysis depending on the application.
- The requirement for a differential amplifier between the THA and the ADC is an inconvenience. A nice feature would be a built-in THA post amplifier with adjustable gain, so noise and linearity can be traded. Even better is to have all of the above (THA, Diff-Amp, and ADC) in one chip.
- As of this writing, Rockwell Scientific has released the RTH020 [10] which is a slightly improved version of the RTH010. Measurement of the RTH020 may be a worthwhile task.

References

- [1] “Low Cost Digital Radar for Fuzing, Tags, SAR Imaging, and Targeting,” Sandia National Laboratories LDRD Proposal 01-0643, June, 2000.
- [2] RTH010 Track-and-Hold Amplifier Data Sheet, Rev E, Rockwell Scientific, Inc.
- [3] E5500A/B Phase Noise Measurement System Users Guide, P/N E5500-90004, Rev A.01.05, Agilent Technologies, June, 2000.
- [4] Brock, Billy C., “The Role of Noise in Analog-to-Digital Converters”, Sandia National Laboratories Report, SAND96-2697, November 1996.
- [5] RAD020 Analog-to-Digital Converter Preliminary Specification, Rev B, Rockwell Scientific, Inc.
- [6] AD8350 Low Distortion, 1.0 GHz Differential Amplifier Data Sheet, Rev A, Analog Devices, Inc., 2001.
- [7] MAX108 Analog-to-Digital Converter Data Sheet, Rev 0, Maxim Integrated Products, Inc., Sept., 1999.
- [8] Matlab Technical Computing Language, Release 12.1, The Mathworks, Inc., May, 2001.
- [9] Doerry, Armin W., “ADC Strobe Timing Jitter,” part of “Lynx SAR: Issues, Analysis, and Design, Part 1,” SAND97-2383/1, Sandia National Laboratories, October, 1997.
- [10] RTH020 Track-and-Hold Amplifier Data Sheet, Rev C, Rockwell Scientific, Inc.
- [11] Stimson, George W., “Introduction to Airborne Radar,” 2nd Edition, SciTech Publishing, Inc., 1998.
- [12] Curlander, John C. and McDonough, Robert N., “Synthetic Aperture Radar, Systems and Signal Processing,” John Wiley & Sons, 1991.
- [13] Sullivan, Roger J., “Microwave Radar, Imaging and Advanced Concepts,” Artech House, 2000.

Matlab Scripts

The following Matlab programs were used to collect and analyze the data for the discrete-time measurements of section 4.2.

DEMO_ADC_ACCUM_RUN.M	{accumulated ADC vector acquisition}
ADC_SINE_TEST.M	{PSD, harmonic, SNR, etc. analysis}
GPIB_SOURCE	{GPIB source control}
RAM_CONFIG.M	{FPGA RAM configuration}
ADC_ACCUMULATOR.M	{accumulate ADC vector}
POWER_SWEEP_THA_ADC.M	{swept THA input power measurement}
FREQ_SWEEP_THA_ADC.M	{swept THA input frequency measurement}
THA_ADC_AMP_VS_FREQ.M	{broadband THA frequency sweep}

FPGA Bit File

FPGA program file drx_fpga55.bit was used for all ADC data acquisitions for the discrete-time measurements.

DISTRIBUTION
Unlimited Release

1	MS0525	K. O. Wessendorf	1732
3	MS0874	T. L. Hardin	1751
1	MS0874	D. Greenway	1751
1	MS0874	D. W. Palmer	1751
1	MS0874	C. E. Sandoval	1751
1	MS0874	M. Armendariz	1751
1	MS0874	P. J. Robertson	1751
1	MS0537	R. E. Heintzleman	2333
1	MS0501	J. D. Bradley	2338
1	MS0505	P. A. Dudley	2341
1	MS0505	D. N. Urenda	2341
1	MS0505	D. K. Werling	2341
1	MS0505	C. K. Wojahn	2341
1	MS0519	D. L. Bickel	2344
1	MS0519	J. T. Cordaro	2344
1	MS0519	A. W. Doerry	2344
1	MS0519	J. J. Mason	2344
1	MS0519	M. S. Murray	2344
1	MS0519	R. C. Ormesher	2344
1	MS0529	K. W. Sorensen	2345
1	MS0529	J. G. Baldwin	2345
1	MS0529	B. C. Brock	2345
1	MS0529	G. G. Delaplain	2345
4	MS0529	D. F. Dubbert	2345
1	MS0529	J. T. Fuller	2345
1	MS0529	F. E. Heard	2345
1	MS0529	R. B. Hurley	2345
1	MS0529	G. R. Sloan	2345
1	MS0529	C. W. Ottesen	2346
1	MS0519	B. L. Remund	2348
1	MS0519	T. P. Bielek	2348
1	MS0519	S. M. Devonshire	2348
1	MS0519	A. L. Navarro	2348
1	MS0519	K. R. White	2348
1	MS1207	N. E. Doren	5912
1	MS9018	Central Technical Files	8945-1
2	MS0899	Technical Library	9616
1	MS0612	Review & Approval Desk for DOE/OSTI	9612
3	Ron Latreille	Rockwell Scientific, Inc. 1049 Camino Dos Rios Thousand Oaks, CA 91360	